New U-Pb age constraints for the Laxford Shear Zone, NW Scotland: Evidence for tectono-magmatic processes associated with the formation of a Paleoproterozoic supercontinent.

K.M. Goodenough[1,*], Q.G. Crowley[2,3], M. Krabbendam[1], and S.F. Parry[4]

1: British Geological Survey, West Mains Road, Edinburgh EH9 3LA, UK

2: NERC Isotope Geosciences Laboratory, Keyworth, Nottingham, NG12 5GG, UK

3: Department of Geology, School of Natural Sciences, Trinity College, Dublin 2, Ireland

4: British Geological Survey, Keyworth, Nottingham, NG12 5GG, UK

* Corresponding author: kmgo@bgs.ac.uk, +44 131 6500272

Abstract

The Lewisian Gneiss Complex in north-west Scotland is a part of the extensive network of Archaean cratonic areas around the margins of the North Atlantic. It is considered to be made up of a number of terranes with differing protolith ages, which have been affected by a range of different metamorphic events. A major shear zone, the Laxford Shear Zone, forms the boundary between two of these terranes. New dates presented here allow us to constrain the timing of terrane assembly, related to the formation of Palaeoproterozoic supercontinents. Early deformation along the Laxford Shear Zone, and primary accretion of the two terranes, occurred during the Inverian event at c. 2480 Ma. This was followed by extension and the intrusion of the mafic Scourie Dykes. Subsequently, renewed silicic magmatic activity occurred at c. 1880 Ma, producing major granite sheets, considered to have formed as part of a continental arc. A further collisional event began at c. 1790 Ma and was followed by slow

exhumation and cooling. This Laxfordian event caused widespread crustal melting, metamorphism and deformation, and is considered to represent the final assembly of the Lewisian Gneiss Complex within the major supercontinent of Columbia (or Nuna).

Keywords

Lewisian Gneiss Complex; Laxfordian; shear zone; geochronology

1 Introduction

The Lewisian Gneiss Complex of north-west Scotland is a fragment of Archaean crust, variably reworked during the Proterozoic. The bulk of its outcrop lies within the foreland to the Caledonian Orogen, and has been largely unaffected by Phanerozoic deformation and metamorphism. It is thus an easily-accessible, well-mapped area in which to study problems of Precambrian crustal evolution.

The Lewisian Gneiss Complex outcrops across two main areas: the islands of the Outer Hebrides, and a broad strip along the north-west coast of mainland Scotland (Figure 1). The whole complex shares the same basic geological history, as established by Sutton and Watson (1951). This history begins with the formation of voluminous tonalite-trondhjemite-granodiorite (TTG) gneisses in a number of Archaean magmatic events, followed by heterogeneous late-Archaean deformation and metamorphism. During the early Palaeoproterozoic, a swarm of mafic dykes (the Scourie Dyke Swarm) was intruded into this Archaean basement. Some parts of the Lewisian were subsequently affected by Palaeoproterozoic reworking.

This history encompasses a complex sequence of metamorphic, magmatic and deformational events that have affected different parts of the Lewisian Gneiss Complex. Early field work showed that some areas of TTG gneisses contained pyroxene (granulite-facies gneisses) whilst others were amphibole-bearing (amphibolite-facies gneisses). On the mainland, a central district of granulite-facies gneisses was mapped out, flanked by northern and southern districts of amphibolite-facies gneiss (Peach et al., 1907). It was subsequently suggested that the entirety of the Lewisian Gneiss Complex had been affected by a granulite-facies ('Scourian') event prior to the emplacement of the Scourie Dykes, whereas only some areas had been affected by a post-Scourie Dyke, amphibolite-facies, 'Laxfordian' event (Sutton and Watson, 1951). Subsequent work recognised an amphibolite-facies, pre-Scourie Dyke event termed the 'Inverian' that formed localised shear zones (Evans, 1965). The early granulite-facies event was renamed from 'Scourian' to 'Badcallian' by Park (1970), to avoid any confusion in terminology. Modern interpretations of the Lewisian Gneiss Complex continue to use this framework of 1) a pre-Scourie Dyke, granulite-facies Badcallian event; 2) a pre-Scourie Dyke, amphibolite-facies Inverian event; and 3) a post-Scourie Dyke, amphibolite-facies Laxfordian event - although the Laxfordian may be divisible into more than one discrete episode, and granulite-facies metamorphism may have occurred at different times in different terranes (Kinny et al., 2005).

Bowes (1962, 1968) proposed that the Badcallian event may not have affected the whole of the Lewisian Gneiss Complex. This view was not widely accepted, and at the time the Lewisian was generally viewed as a single block of crust which had been affected by the same tectonic events – albeit with juxtaposition of different crustal levels along shear zones to create the heterogeneous patterns of metamorphism and deformation (Park and Tarney, 1987).

As modern geochronological techniques began to be applied during the 1980s and 1990s, it became clear that the Lewisian gneisses were not all derived from protoliths of the same age (Whitehouse, 1989, Kinny and Friend, 1997). This led to the development of a terrane model, in which the Lewisian Gneiss Complex is considered to be made up of several different crustal blocks that had different histories up until the point when they were juxtaposed into their present relative positions (Friend and Kinny, 2001, Kinny et al., 2005). This concept is now broadly accepted, although debate continues about the number of component terranes, the position of their boundaries, and the nature and timing of their accretion (Mason and Brewer, 2005, Park, 2005, Goodenough et al., 2010, Love et al., 2010).

One of the best candidates for a terrane boundary in the Lewisian is the Laxford Shear Zone, in the northern part of the mainland outcrop. This paper presents new U-Pb geochronological data for rocks from this shear zone, and provides new information about the timing of terrane accretion in the north of the Lewisian Gneiss Complex. Two separate Palaeoproterozoic magmatic events are recognised, and can be correlated with widespread activity across a Palaeoproterozoic supercontinent.

2 The geology of the Laxford Shear Zone

The Laxford Shear Zone (LSZ) runs through Loch Laxford, in the mainland outcrop of the Lewisian Gneiss Complex (Figure 1). It is a major polyphase shear zone, some 8 km wide and WNW-trending (Coward, 1990), which separates amphibolite-facies gneisses to the north from granulite-facies gneisses to the south. The northern, amphibolite-facies district has been termed the Rhiconich terrane, whilst the central granulite-facies district, south of the LSZ, has been named the Assynt terrane (Friend and Kinny, 2001). The field relationships around the LSZ have been described in detail elsewhere (Goodenough et al., 2010) and are briefly summarised here.

The lithologies to the south of the Laxford Shear Zone, around Scourie (Figure 2), are banded, grey, pyroxene-bearing TTG gneisses of the Assynt terrane, with mafic to ultramafic lenses and larger masses varying from a few cm to 100s of metres in size. The gneissic banding generally dips gently towards the WNW. Locally, the gneisses and mafic-ultramafic bodies are cut by thin (5 cm – 5 m) coarse-grained to pegmatitic granitoid sheets that are foliated, but cut the gneissic banding (Evans and Lambert, 1974, Rollinson and Windley, 1980). All these lithologies are cut by NW-SE trending Scourie Dykes, typically 5-50 m wide. The area is transected by discrete east-west amphibolite-facies shear zones, generally a few metres wide, which deform and offset the dykes and are thus demonstrably Laxfordian in age. Approaching the LSZ, these shear zones increase in abundance and swing into a NW-SE orientation.

The southern margin of the LSZ is marked by the incoming of a steeply SW-dipping (50°-70°), pervasive foliation in the gneisses, which has been formed by the thinning of the original gneissic banding. This foliation is axial planar to folds of the gneissic banding, and those folds are cross-cut by Scourie Dykes (Beach et al., 1974). The foliation is thus considered to be Inverian in age, and to represent the first stage of deformation in the Laxford Shear Zone. Discrete Laxfordian shear zones, generally less than 100 m in width, are superimposed upon this Inverian structure. They are usually only identified where they cut Scourie Dykes, which post-date the Inverian deformation, but were deformed during the Laxfordian.

Within the LSZ lies a 1-2 km thick zone dominated by mafic-ultramafic lithologies (‘early mafic gneisses’), associated with brown-weathering, garnet-biotite semi-pelitic schists that are considered to be metasedimentary in origin (Davies, 1974, Davies, 1976). These were metamorphosed and deformed during both the Badcallian and Inverian events, as were metasedimentary gneisses in a similar structural setting at Stoer, further south in the Assynt terrane, (Zirkler et al., 2012). The zone of early mafic and metasedimentary gneisses in the LSZ extends for some 15 km, from the coast on the SW side of Loch Laxford in the west to Ben Stack in the east (Figure 2). Many of the mafic rocks are garnet-bearing amphibolites, some of which contain relict granulite-facies assemblages and evidence for Badcallian partial melting (Johnson et al., 2012), and they were deformed and foliated during the Inverian event (Davies, 1974). The mafic-ultramafic-metasedimentary association is considered to be part of the Assynt terrane, but its original relationship with the surrounding TTG gneisses is not clear. This belt is cross-cut by Scourie Dykes, and also by scattered sheets of unfoliated granite and granitic pegmatite that formed during the Laxfordian event (Goodenough et al., 2010). Discrete Laxfordian shear zones are common in this area, but again are only easily recognised where they affect Scourie Dykes.

To the north of the belt of mafic rocks, the grey TTG gneisses of the Assynt terrane rapidly give way to migmatitic, granodioritic gneisses with abundant sheets and veins of granite and granitic pegmatite. These migmatitic gneisses belong to the Rhiconich terrane. Within this area, Scourie Dykes are folded, foliated and cross-cut by the granitic sheets (Goodenough et al., 2010). The main magmatic and deformational event in these migmatitic gneisses is thus considered to be Laxfordian in age, but the Laxfordian fabric is essentially parallel to – and superimposed upon – the Inverian foliation in the southern part of the LSZ.

The boundary between the two terranes is rather variable in character along its length and can be difficult to identify (Goodenough et al., 2010). In some areas it appears to be sharp, with mafic-ultramafic rocks in the Assynt terrane being separated by a narrow, discrete shear zone from migmatitic gneisses of the Rhiconich terrane; in other places, it lies within the felsic gneisses, and is thus difficult to locate. East of Loch Laxford, this boundary is obscured by thick (up to 100 m) weakly foliated granitic sheets, which cross-cut the gneissic banding at a low angle.

The northern margin of the Laxford Shear Zone has generally been placed around Laxford Bridge (Figure 2; Beach et al., 1974), but no sharp boundary exists, and Coward (1990) has described the area north of Laxford Bridge as ‘a gently dipping Laxfordian shear zone’. In summary, the LSZ can be considered as an Inverian shear zone marking the line of juxtaposition of the Assynt and Rhiconich terranes. It was reactivated during the Laxfordian, when the more hydrous, fusible gneisses of the Rhiconich terrane partially melted and were pervasively deformed, whilst the brittle, dry gneisses of the Assynt terrane were only deformed along discrete shear zones (Goodenough et al., 2010).

3 Previous geochronological work

The rocks of the Lewisian Gneiss Complex around the Laxford Shear Zone have been the subject of a number of geochronological studies, the majority of which have focused on the protolith and metamorphic ages of the TTG gneisses. The earliest work made use of the Rb-Sr and K-Ar chronometers (Holmes et al., 1955, Giletti et al., 1961). Pegmatites from within the Assynt terrane, which are cut by Scourie Dykes, were dated 'as at least 2460 Ma', whilst the Laxfordian metamorphism was placed at 'about 1600 Ma' (Giletti et al., 1961). These early radiometric age constraints were remarkably accurate for the time, and thus the broad chronology of the Lewisian gneisses has been known for some 50 years.

Early Pb-Pb isotope work was interpreted to show that U depletion in the gneisses had occurred at around 2900 Ma, and was assumed to be related to the Badcallian metamorphism (Moorbath et al., 1969). Subsequent work with Sm-Nd isotopes refined this to give protolith ages for the Lewisian gneisses of around 2950 Ma (Hamilton et al., 1979, Whitehouse and Moorbath, 1986), whilst the Badcallian metamorphism was dated at 2660 to 2700 Ma using U-Pb in zircon (Pidgeon and Bowes, 1972, Chapman and Moorbath, 1977, Cohen et al., 1991). The Scourie Dykes were dated at 2000-2400 Ma using U-Pb techniques on baddeleyite (Heaman and Tarney, 1989). Rb-Sr and K-Ar dating of samples from the Laxford Shear Zone indicated that the 'climax' of the Laxfordian metamorphism occurred at approximately 1850 Ma (Lambert and Holland, 1972), followed by relatively slow cooling.

Until the 1990s, it was considered that these dates could be extrapolated across the whole of the Lewisian Gneiss Complex.

The development of high-precision U-Pb techniques for dating accessory minerals such as zircon, and the ability to date individual crystals, or domains within crystals, revolutionised dating of the Lewisian Gneiss Complex and revealed a level of chronological detail that matches the complexity of observed field relationships. Protolith ages of TTG gneisses in the Assynt terrane were shown to be c. 2960 Ma (Friend and Kinny, 1995), whilst gneisses in the Rhiconich terrane have yielded younger protolith ages of c. 2840-2800 Ma and also record magmatism at 2680 Ma (Kinny and Friend, 1997). Two high-grade metamorphic events were recognised in gneisses of the Assynt terrane, the first at c. 2760 Ma (Corfu et al., 1994, Zhu et al., 1997), and the second at c. 2490-2480 Ma (Whitehouse and Kemp, 2010, Corfu et al., 1994, Friend and Kinny, 1995, Kinny and Friend, 1997)). These two metamorphic events were correlated with the Badcallian and Inverian, respectively, by Corfu et al. (1994). Neither event was recognised in zircon from the Rhiconich terrane gneisses (Kinny and Friend, 1997). Dating of titanites and monazites provided an age of c. 1750 Ma for the Laxfordian metamorphism in both the Assynt and Rhiconich terranes, with a later phase of hydrothermal activity at c. 1690-1670 Ma (Corfu et al., 1994; Zhu et al., 1997; Kinny and Friend, 1997).

The evidence for different protolith ages to the north and south of the Laxford Shear Zone, together with the apparent lack of high-grade metamorphic events recorded in the Rhiconich terrane, led Kinny and Friend (1997) to propose that the two blocks were in fact separate terranes. They were considered to have had separate histories until their juxtaposition during the Laxfordian event. Friend and Kinny (2001) suggested that Laxfordian granitic sheets are only found in the Rhiconich terrane. They dated one of these sheets at c. 1854 Ma, and thus proposed that the juxtaposition of the two terranes occurred after that date. However, Goodenough et al. (2010) showed that the granitic sheets in fact ‘stitch’ the Laxford Shear

Zone, and are found within the Assynt terrane. The Laxford Shear Zone, which marks the terrane boundary, is a major Inverian shear zone upon which Laxfordian shearing has been superimposed, and thus the field relationships indicate that the terranes were juxtaposed during the Inverian event (Goodenough et al., 2010).

The absolute age of the Inverian event remains a matter of debate. This event is defined on the basis of field relationships as the amphibolite-facies metamorphism and deformation which post-dates the granulite-facies metamorphism in the Assynt terrane, but pre-dates the Scourie Dykes (Evans, 1965; Evans and Lambert, 1974). It is not recognisable in the field in the Rhiconich terrane, but this may be due to the intensity of later Laxfordian deformation. A suite of pegmatites found in the Lochinver and Scourie areas is unaffected by Badcallian deformation and metamorphism, but is deformed in Inverian shear zones, and has generally been considered to have formed at an early stage in the Inverian event (Evans and Lambert, 1974, Tarney and Weaver, 1987, Corfu et al., 1994). These pegmatites have been dated at c. 2480 Ma (Corfu et al., 1994; Zhu et al., 1997). Although interpretation of Lewisian zircon is certainly not straightforward, many authors have placed the Badcallian high-grade metamorphic event at c. 2700 – 2800 Ma, which would fit with an Inverian event at c. 2480 Ma (Corfu et al., 1994; Zhu et al., 1997; Whitehouse and Kemp, 2010). An alternative view suggests that high-grade metamorphism affected the Assynt terrane at c. 2490 - 2480 Ma and that this equates to the Badcallian (Love et al., 2004, Kinny et al., 2005), which would place the Inverian in the interval between c. 2480 Ma and the oldest Scourie Dyke at c. 2400 Ma (Heaman and Tarney, 1989).

Recent detailed mapping of the Laxford Shear Zone has allowed clear identification of structures and intrusions formed during the Inverian and Laxfordian events (Goodenough et al., 2010). Samples from well-characterised outcrops were collected for radiometric dating, in order to constrain the timing of the Inverian and Laxfordian events, and their related magmatism. The sample localities are indicated on Figure 2, and briefly described below.

4 Sample localities

4.1 Badnabay

The belt of mafic-ultramafic and metasedimentary gneisses, which forms the northern margin of the Assynt terrane, is well exposed around 1 km south of Badnabay, on the south side of Loch Laxford. The gneisses around Badnabay itself are migmatitic quartzofeldspathic gneisses, containing abundant granitic veins and sheets, and belong to the Rhiconich terrane. To the south, these pass into well-banded hornblende-bearing tonalitic gneisses of the Assynt terrane, although a sharp contact cannot be mapped out between the two gneiss types. Around [NC 216 457], the tonalitic gneisses are in contact with brown-weathering garnet-biotite schists and coarse-grained garnet amphibolite, which belong to the main mafic-ultramafic-metasedimentary belt. The garnet amphibolites of this belt locally contain remnant two-pyroxene assemblages and evidence for partial melting, and so the belt is considered to have been metamorphosed to granulite facies during the Badcallian (Johnson et al., 2012). All the lithologies carry a strong NW-SE-trending, steeply-dipping foliation and an ESE-plunging lineation. These structures are cut by Scourie Dykes along strike, and are thus attributed to the Inverian. The metasedimentary rocks and tonalitic gneisses are cut by an irregular, anastomosing coarse-grained granitic sheet, 1-5 m thick, which is undeformed. This represents one of the most southerly Laxfordian granites within the Assynt terrane.

Sample LX1 was collected from the granite sheet at [NC 21679 45741]. It is a medium- to coarse-grained, fairly equigranular, two-feldspar biotite-muscovite granite. Sample LX2 was collected from the metasedimentary biotite schists at [NC 21638 45754]. It is a medium-grained, strongly recrystallised garnetiferous semi-pelite, comprising quartz, plagioclase, biotite and garnet.

4.2 Tarbet

The traverse from the coastal village of Tarbet to Rubha Ruadh on the south shore of Loch Laxford is considered to be the classic section through the Laxford Shear Zone (Beach, 1978). At [NC 16379 49320], hornblendic mafic gneisses of the Assynt terrane are cut by numerous thin (up to 50 cm), pink microgranitic sheets. Both gneisses and microgranitic sheets carry a strong NW-SE trending, steeply dipping foliation and are folded into tight upright folds that are axial planar to the foliation (Figure 3a). The foliation is considered to be Inverian in age, on the basis of relationships with Scourie Dykes along strike. It is possible that a component of Laxfordian deformation has been superimposed on the main Inverian fabric, but cannot be distinguished here. Some 15 m to the west, the Inverian foliation is locally cross-cut by sheets of undeformed pink coarse-grained Laxfordian granite. Sample LX11 was collected from a thin, folded, foliated microgranite sheet that was clearly affected by Inverian deformation. The microgranite is medium-grained, with a foliation defined by ribbons of recrystallised quartz separated by zones of sericitised alkali feldspar + quartz + muscovite + biotite.

4.3 Ben Stack

On the north side of Ben Stack, thick (up to 100 m) sheets of foliated, medium- to coarse-grained granite are intruded along the boundary between the Assynt and Rhiconich terranes. On a map scale, these granite sheets cross-cut the Inverian foliation, but they were themselves weakly deformed during the Laxfordian event. They contain relatively small amounts (~ 15% of the rock) of mafic minerals that include alkali amphibole and alkali pyroxene. Mineral phases such as these are unlikely to have crystallised from the peraluminous melts that would be derived by melting of the local crust alone (Watkins et al., 2007). These granite sheets therefore represent the addition of at least a component of juvenile magma to the crust. Sample LX6 was collected from one of these thick granite sheets at [NC 26050 43696]. It is a medium- to coarse-grained, equigranular granite with a weak foliation defined by aligned mafic mineral phases. The mineralogy comprises quartz, alkali feldspar, plagioclase, aegirine, and an alkali amphibole, with abundant accessory titanite as well as zircon and monazite. The granite has been recrystallised and foliated after emplacement, but with little or no new mineral growth, although titanites show evidence of some alteration and late overgrowths.

4.4 Rhiconich

Around the village of Rhiconich, migmatitic gneisses typical of the Rhiconich terrane are exposed. These gneisses are intruded by abundant, irregular, undeformed granitic sheets and pegmatites that cross-cut the banding in the gneisses (Figure 3b). The main mafic minerals in these granites are chlorite and muscovite, and field relations indicate that these granites may have been largely derived by melting of local crust, although experimental data suggest that an additional component of melt may have been required to produce the more potassic granites (Watkins et al., 2007). Foliated amphibolites in this area, which are considered to be members of the Scourie Dyke Swarm, are also cut by the granitic sheets. The pervasive deformation of these Scourie Dykes indicates that the whole area was affected by Laxfordian deformation. In contrast, the granitic sheets are undeformed, and therefore were intruded at a relatively late stage in the Laxfordian event. Sample LX7 was collected from one such granitic pegmatite sheet in a road cutting at [NC 24645 51912]. The sample is very coarse-grained, being largely made up of quartz and alkali feldspar with abundant evidence of recrystallisation along grain boundaries. Chlorite (after biotite) and muscovite form <10% of the rock.

5 Methodology and analysis

Individual samples of approximately 5 kg of fresh, unaltered material were crushed and sieved using standard mineral preparation procedures. Heavy minerals were concentrated using a Wilfley table prior to gravity settling through methylene iodide for separation of the heavy mineral concentrate, which was subsequently washed in acetone and dried. Zircons, titanites and monazites were separated initially by paramagnetic behaviour using a Franz isodynamic separator and then hand-picked from the non-magnetic and least magnetic fractions.

5.1 Laser-ablation Multicollector Inductively Coupled Plasma Mass Spectrometry (LA-MC-ICP-MS)

LA-MC-ICP-MS U-Pb geochronology was performed at the NERC Isotope Geosciences Laboratory (UK). Mineral separates were mounted in an araldite resin block, ground to near mid-thickness and polished. Cathodoluminescence (CL) images of zircon grains (Figure 4) were acquired at the British Geological Survey using an FEI QUANTA 600 Environmental Scanning Electron Microscope (tetrode tungsten gun version) equipped with a KE Developments Centaurus Cathodoluminescence Detector, and these were used to select target spots for analysis. Analyses used a Nu Plasma MC-ICP-MS system coupled to a New Wave Research 193nm Nd:YAG LA system. A laser spot size of 25 microns was used to ablate discrete zones within grains. The total acquisition cycle was about one minute, which equates to approximately 15µm depth ablation pits. A $^{205}Tl/^{235}U$ solution was simultaneously aspirated during analysis using a Cetac Technologies Aridus desolvating nebulizer to correct for instrumental mass bias and plasma induced inter-element fractionation. Data were collected using static mode acquiring ^{207}Pb, ^{206}Pb and ^{204}Pb&Hg in ion counting detectors. A common-Pb correction based on the measurement of ^{204}Pb was attempted, but interference from the ^{204}Hg peak overwhelmed the common-Pb contribution from the zircon grains. As a result of this, data presented are non-common Pb corrected. Analyses with high common Pb (^{204}Pb cps in excess of 200cps) were rejected, but these amounted to a <0.5% of the total data set and were not disproportionately from any one sample. Some minor elevation in common Pb may be responsible for generating excess scatter in the calculated weighted mean ^{207}Pb/^{206}Pb ages. Data were normalised using the zircon standard 91500 whereas two additional zircon standards (GJ-1 and Mud Tank) were treated as unknown samples to monitor accuracy and precision of age determinations. During the various analytical sessions secondary standards produced values within error of published ages. GJ-1 gave a Concordia age of 607.1 ± 2.7 Ma (reported TIMS ^{207}Pb/^{206}Pb is 608.5 ± 0.4 Ma (Jackson et al., 2004)), and Mud Tank gave a Concordia age of 733.3 ± 3.7 Ma (TIMS age 732 ± 5 Ma (Black and Gulson, 1978)). Raw measured intensities of ^{204}Pb for these secondary standards did not deviate significantly from those of the unknowns, indicating that the treatment of non-common Pb data produces ages within error of TIMS common-Pb corrected data. Data were reduced and errors propagated using an in-house spreadsheet calculation package, with ages determined using the Isoplot 3 macro of Ludwig (2003). Uncertainties for each ratio are propagated relative to the respective reproducibility of the standard, to take into account the errors associated with the normalisation process and additionally to allow for variations in reproducibility according to count rate of the less abundant ^{207}Pb peak. All ages are reported at the 2σ level. A full description of analytical protocols can be found in Thomas et al. (2010). Data are presented in tables 1 and 3-7.

5.2 Thermal Ionization Mass Spectrometry (TIMS)

Dating of selected samples was conducted by isotope dilution thermal ionization mass spectrometry (ID-TIMS) in order to produce higher precision data and to provide independent verification of LA-MC-ICP-MS data. Zircon was thermally annealed and leached by a process modified from that of Mattinson (Mattinson, 2005). Zircon grains from individual samples were annealed as bulk fractions at 850^{o}C in quartz glass beakers for 60 hours. Once cooled, the zircon grains were ultrasonically washed in 4N HNO_3, rinsed in ultra-pure water, then further washed in warm 4N HNO_3 prior to rinsing with water to remove surface contamination. The annealed and cleaned zircon fractions were then chemically leached in Teflon microcapsules enclosed in a Parr bomb using 200µl 29N HF and 20µl 8N HNO_3 at 180^{o}C for 12 hours to minimise or eliminate damaged zones in which Pb loss may have occurred. TIMS data are presented in table 2.

A mixed ^{205}Pb – ^{233}U – ^{235}U EARTHTIME tracer was used to spike all fractions, which once fully dissolved, were converted to chloride and loaded onto degassed rhenium filaments in silica gel, following a procedure modified after Mundil et al. (2004). A Thermo Electron Triton at NIGL was used to collect all U-Pb TIMS data. Approximately 100 to 150 ratios of Pb isotopic data were dynamically collected using a MassCom Secondary Electron Multiplier (SEM). Between 60 and 80 ratios were statically collected using either a SEM or Faraday cups for U, depending on signal strength. Pb ratios were scrutinised for any evidence of organic interferences using an in-house raw ratio statistical and plotting software, but these were found to be negligible or non-existent. Errors were calculated using numerical error propagation (Ludwig, 1980). Isotope ratios were plotted using Isoplot version 3.63 (Ludwig, 1993, Ludwig, 2003); error ellipses on concordia diagrams reflect 2σ uncertainty. Total procedural blanks were 1.0 pg for Pb and c. 0.1 for U. Samples were blank corrected using the measured blank composition. Correction for residual common lead above analytical blank was carried out using the Stacey-Kramers common lead evolutionary model (Stacey and Kramer, 1975).

6 Results

6.1 Badnabay

Two distinct morphological types of zircon were separated from sample LX1, the undeformed granite cutting mafic gneisses and metasedimentary rocks within the Laxford Shear Zone. Small, acicular zircon grains (c. 80x30x20 µm), interpreted as igneous in origin using CL imaging, were dated using ID-TIMS. Three single grain fractions form a cluster on concordia with a mean $^{207}Pb/^{206}Pb$ age of 1773.1 ± 1.1Ma (Figure 5a). One discordant fraction shows evidence of Pb-loss evidently not removed by the chemical abrasion procedure. Larger (c. 150x120x120 µm), multi-faceted zircon grains from the same sample (Figure 4) were dated using LA-ICPMS. Overgrowths identified in CL images and interpreted as igneous in origin give a mean $^{207}Pb/^{206}Pb$ age of 1774 ± 5.6 Ma (Figure 5b), within error of the ID-TIMS age on acicular zircon from the same sample. Analyses of inherited cores from multi-faceted zircon give a range of ages, in excess of c. 2558 Ma. The ID-TIMS age of 1773.1 ± 1.1 Ma is taken as the best estimate for the intrusive age of this granite sheet.

Zircon from the metasedimentary biotite schist, sample LX2, was dated using LA-ICPMS. Zircon grains from this sample vary from c. 300x150x150 to 150x100x100 µm, typically with ovoid morphologies characteristic of detrital grains. CL images of these grains reveal subtle metamorphic textures such as net-veining and patchy growth zonation (Figure 4). The analyses give a range of ages from c. 2475 Ma to 2784 Ma (Figure 5c). Although there is a cluster of analyses at c. 2685 Ma, it is not possible to recognise statistically coherent age groups within the dataset, as the analyses plot along concordia within the age range. The ages determined for this sample are not considered to represent true detrital ages, but are interpreted to have been affected by partial resetting due to granulite-facies metamorphism and/ or Pb-loss, and therefore cannot be used to infer a maximum depositional age for the original sedimentary rocks. This interpretation of metamorphic resetting is consistent with the relict granulite-facies mineral assemblage and evidence for partial melting in the associated mafic-ultramafic rocks (Johnson et al., 2012), and field evidence for deformation and metamorphism during the Inverian event. The youngest ages (c. 2475 Ma) are considered to approximate to the timing of the Inverian event, after which the zircon systematics were not disturbed.

6.2 Tarbet

Zircon grains from sample LX11, the folded and foliated microgranite, are typically c. 400x200x200 to 250x150x100 µm. They have abundant, large igneous oscillatory zoned cores with igneous oscillatory zoned overgrowth patterns of variable width, and narrow (2-30 µm), bright CL rims (Figure 4). The latter are consistent with a metamorphic origin or some disturbance of the zircon lattice structure due to deformation assisted fluid infiltration. The majority of analyses from this sample are slightly discordant (1-6%) (Figure 5d). A discordia through 54 out of the total of 69 analyses for this sample (15 analyses were excluded for lying off the main discordia trajectory) yields an upper-intercept age of 2843 ± 33 Ma and a lower-intercept age of c. 1750 Ma (Figure 5d). Note that only one analysis lies close to c. 1750 Ma, hence the poorly constrained lower-intercept age. A number of analyses (n=11) lie on a mixing chord between c. 2480 Ma and >2850 Ma, suggesting that a c. 2480 Ma event also affected the zircon from this sample. Given the width of the bright CL rims, it was difficult to avoid ablating a mixture of rim and igneous zircon, so a number of analyses represent a mixture of older igneous growth (possibly both c. 2843 and c. 2480 Ma) and younger rims (c. 1750 Ma). It is difficult to place an unequivocal interpretation on these complex data, but we suggest that the c. 2843 Ma age represents the protolith age of the country rock gneisses, which were subsequently partially melted to form the granite sheets during metamorphism and deformation at c. 2480 Ma, with subsequent metamorphism at c. 1750 Ma.

6.3 Ben Stack

Zircon and titanite were recovered from sample LX6, taken from the thick granite sheet on the north side of Ben Stack. Zircon grains typically are 300x250x200 to 200x100x100 µm, with some oscillatory zonation evident in CL. Patchy, dull and net-veined CL patterns and obvious inherited cores also exist in many zircon grains from this sample (Figure 4). Titanite grains are large, up to 1 mm in length, with some evidence of alteration and late overgrowths. Both zircon and titanite were dated by LA-ICPMS. U-Pb zircon analyses plot along concordia, mainly between c. 1880 and 2765 Ma (Figure 6a). A frequency probability plot of all the zircon LA-ICPMS data for LX6 shows a dominant peak at c. 1880 Ma, with a subordinate peak at c. 2480 to 2500 Ma (Figure 6b). A weighted mean $^{207}Pb/^{206}Pb$ age of the main population gives 1880.1 ± 4.2 Ma (Figure 6c). Apparent ages intermediate between c. 2765-2500 Ma and 1883-2480 Ma are most likely analytical artefacts of mixing by ablating different age domains. The age of 1880.1 ± 4.2 Ma is taken as the best estimate for emplacement of this granite body, with older ages representing abundant inherited grains.

Titanite analyses have variable amounts of common Pb. When all titanite LA-ICPMS analyses are plotted on a Tera Wasserburg diagram, they fall along a discordia with a lower intercept at 1671 + 12/ -11 Ma (Figure 6d). It is possible that there are two separate trajectories on this diagram, indicating that there may be more than one titanite age present in this sample, but this is not resolvable as the analyses are within analytical uncertainty. The age of 1671 +12/-11 Ma is considered to be a cooling age for titanite.

6.4 Rhiconich

Zircon from sample LX7, the granite sheet from the Rhiconich terrane, was dated using LA-ICPMS. Zircon grains are typically 400x200x150 to 150x75x50 µm with abundant inherited cores visible in CL images (Figure 4). A concordia diagram (Figure 6e) shows a cluster of analyses at c. 1790 Ma and older ages between c. 2550 and 2860 Ma. A weighted mean $^{207}Pb/^{206}Pb$ age of the four least discordant analyses from the younger main age population gives 1792.9 ± 3.0 Ma, (Figure 6f) which is taken as the best estimate of the intrusion age of the granite. The older dates between c. 2550 and 2860 Ma are interpreted as inherited ages. Two analyses at c. 1980 and 2360 Ma are discordant, and most probably represent mixtures of c. 1790 and > 2500 Ma components.

7 Discussion

7.1 Archaean to earliest Palaeoproterozoic events

Dating of individual metamorphic events within the Lewisian Gneiss Complex has generally proved problematic (e.g. Corfu et al., 1994; Kinny et al., 2005; Whitehouse and Kemp, 2010), as it is generally difficult to clearly relate new zircon growth to either Badcallian or Inverian metamorphism; there is no definitive textural test to distinguish between amphibolite-facies and granulite-facies zircon. However, two samples in this study, the deformed granite from Tarbet (LX11) and the metasedimentary rock from Badnabay (LX2), do show clear field evidence for Inverian deformation.

Field relationships suggest that the thin, deformed microgranitic sheets near Tarbet were probably formed by partial melting of local crustal material, and were intensely deformed and recrystallised during the Inverian and possibly the Laxfordian events. CL images of zircon from this sample show that igneous zircon, dated at 2843 ± 33 Ma, is volumetrically dominant. Bright CL rims are present in zircon from this sample and two separate mixing trajectories may exist, defining two separate lower-intercept ages of c. 2480 and c. 1750 Ma. However, it is not possible to attribute these lower intercept ages to particular rim domains visible in CL. Although this sample locality lies near the northern margin of the Assynt terrane as defined in the field, the inherited protolith age of c. 2843 Ma is within error of those observed for gneisses in the Rhiconich terrane (Kinny and Friend, 1997), and this suggests that the terranes may share more magmatic events than previously thought. The data are best explained by formation of the country rock gneisses at c. 2843 Ma, followed by a metamorphic event at c. 2480 Ma during which partial melting generated the granitic sheets. Metamorphism and deformation during a subsequent event at c. 1750 Ma caused growth of thin rims and disturbance of U-Pb systematics.

The c. 2843 Ma protolith age for the country rock gneisses indicates magmatism within the Assynt terrane at that time. The lower intercept ages, whilst not definitive, indicate a high-temperature metamorphic event at c. 2480 Ma during which the granitic sheets were formed by partial melting. Granitic sheets of this age are only recognised within the Inverian shear zone, and so this event at c. 2480 Ma is most likely to be the Inverian as suggested by a number of authors (Corfu et al., 1994; Zhu et al., 1997; Whitehouse and Kemp, 2010). However, we cannot completely rule out the possibility that the granitic sheets were formed in a Badcallian granulite-facies event at c. 2480 Ma which was immediately followed by the Inverian deformation, and subsequently by a Laxfordian event at c. 1750 Ma.

The metasedimentary sample (LX2) from Badnabay contains zircon with a range of ages which were likely reset by high-grade metamorphism, as demonstrated by metamorphic textures evident in CL imaging and by the spread of analyses overlapping within uncertainty with the concordia curve between c. 2475 and 2784 Ma. On this basis, they cannot be used to provide information about the source of the original sedimentary rocks. The youngest ages from this sample are c. 2475 Ma and we interpret this age as approximating the end of the Inverian event. This age is within error of the lower intercept age of c. 2480 Ma for sample LX11, and indicates that the age of Inverian high-grade metamorphism and deformation in the Laxford Shear Zone was around 2480 Ma.

7.2 Palaeoproterozoic events

The term ‘Laxfordian’ has traditionally been used to describe all events in the Lewisian Gneiss Complex that post-date the Scourie Dykes, but it is becoming clear that this encompasses a whole range of metamorphic and magmatic events (Kinny et al., 2005). This is exemplified by our new U-Pb data (Table 8). The thick foliated granite sheets on the north side of Ben Stack are part of the Rubha Ruadh granite suite of Kinny et al. (2005). These voluminous granites, which intrude the boundary zone between the Assynt and Rhiconich terranes, are associated with an input of juvenile magma into the crust. The new emplacement age of 1880.1 ± 4.2 Ma (sample LX6) is close to the 1854 ± 13 Ma date obtained by Friend and Kinny (2001) from another intrusion in this suite, and our new date for sample LX6 significantly extends the duration of this magmatism.

Magmatism is known to have occurred elsewhere within the Lewisian Gneiss Complex at roughly this time, notably in the South Harris Complex of the Outer Hebrides at c. 1890 Ma (Mason et al., 2004), in the Nis terrane on the Isle of Lewis at c. 1860-1870 Ma (Whitehouse, 1990, Whitehouse and Bridgwater, 2001) and in the Loch Maree Group further south on the mainland at c. 1900 Ma (Park et al., 2001). High-grade metamorphism of similar age has also been recognised in the Ialltaig gneisses, further south in the mainland Lewisian Gneiss Complex (Love et al. 2010), and in the gneisses of South Harris (Whitehouse and Bridgwater, 2001, Friend and Kinny, 2001, Mason, 2012). These ages are generally associated with the development of magmatic arcs which were subsequently accreted and buried by continental collision (Whitehouse and Bridgwater, 2001; Park et al., 2001).

A relatively thin, undeformed granite sheet, cutting the Assynt terrane within the Laxford Shear Zone, has been dated at 1773.1 ± 1.1 Ma (sample LX1). A similar granitic sheet from the Rhiconich terrane has been dated at c. 1793 Ma (sample LX7). Field relationships indicate the likelihood that these granitic sheets were derived by local crustal melting, potentially during an episode of crustal thickening. Although intrusions of this age have not been recorded elsewhere in the Lewisian Gneiss Complex, formation of hydrothermal titanite at >1754 Ma (Corfu et al., 1994) and resetting of earlier formed titanite at c. 1750 Ma (Corfu et al., 1994, Kinny and Friend, 1997) have been recorded in both the Assynt and Rhiconich terranes. Metamorphic rims from deformed granitic sheets in the Laxford Shear Zone also give ages of c. 1750 Ma (sample LX11). U-Pb dating of titanites in the Ben Stack granitic sheet, sample LX6, indicates that these rocks were cooled slowly from their peak temperature, with the titanite cooling through its closure temperature (600-700°C) at c. 1670 Ma. This overlaps within error (1690-1670 Ma) with growth of secondary titanite and rutile considered to be related to low grade alteration and hydrothermal growth of these minerals (Corfu et al 1994). There is no evidence for secondary growth of titanite in sample LX6; the dated titanites appear to be igneous in origin. Taken together, all these ages indicate a long-lived crustal heating event, followed by slow cooling, in the northern part of the Lewisian Gneiss Complex between c. 1790 and c. 1670 Ma – encompassing the events defined as Laxfordian and Somerledian by Kinny et al. (2005). Somerledian ages have been recognised throughout the Lewisian Gneiss Complex (Corfu et al., 1994; Love et al., 2004).

It seems that at least two main magmatic events affected much of the Lewisian Gneiss Complex in the Palaeoproterozoic. The first involved formation of a magmatic arc and introduction of mantle-derived magma in one or more pulses along the margins of the gneiss terranes at c. 1900-1870 Ma. This was followed by a later crustal thickening, heating and melting event which began at c. 1790 Ma and continued, cooling slowly, to c. 1660 Ma. Evidence of these events cannot be used on its own to correlate different terranes or terrane boundaries, since it is now clear that most terranes in the Lewisian Gneiss Complex were affected by these Palaeoproterozoic events.

7.3 Comparison with other North Atlantic cratonic areas

The magmatism that occurred throughout much of the Lewisian Gneiss Complex at c. 1900-1870 Ma and c. 1790 Ma can be related to the development of magmatic arcs and the accretion of an ancient supercontinent (Columbia or Nuna; Zhao et al. (2004), Rogers and Santosh (2002)). This supercontinent incorporated much of the existing crust at that time, and therefore collisional belts of this age are widespread across the globe. Within the British Isles, orthogneisses of similar age (1780 – 1880 Ma; Marcantonio et al. (1988), Daly et al. (1991), McAteer et al. (2010)) are also found in the Rhinns Complex of western Scotland, which extends south-westwards to Ireland.

In southwestern Greenland, along the southern margin of the Archaean craton, the Ketilidian belt contains plutons emplaced in a continental magmatic arc that formed at c. 1854-1795 Ma (Garde et al., 2002a). This was followed by uplift and deformation of the fore-arc at c. 1795-1780 Ma with widespread anatexis and emplacement of S-type granites (Garde et al., 2002b). Similarly, the Nagssugtoqidian orogen to the north of the Greenland Archaean craton contains evidence for arc magmatism at 1940-1870 Ma followed by high-grade metamorphism (Kalsbeek and Nutman, 1996, van Gool et al., 2002, Nutman et al., 2008) with subsequent lower-grade metamorphism at c. 1780-1750 Ma. Palaeoproterozoic accretionary belts of similar age extend westwards into North America, including the Torngat, New Quebec and Trans-Hudson orogens (van Kranendonk et al., 1993, Scott, 1998, St-Onge et al., 2009).

In Scandinavia, the Lapland-Kola Belt also contains juvenile, arc-type magmas of c. 2000-1860 Ma (Daly et al., 2006) although here there is evidence for major crustal shortening and high-grade metamorphism at c. 1950-1870 Ma, rather earlier than is recognised in Scotland. The Svecofennian Orogen is a collage of Palaeoproterozoic, arc-type magmatic units emplaced in two main pulses at 1900 – 1870 and 1830 – 1790 Ma (Lahtinen et al., 2009).

Overall, it is clear that Palaeoproterozoic events in the Lewisian Gneiss Complex can be correlated with those in the surrounding cratonic areas.

8 Refining the model for the Lewisian Gneiss Complex

An overall model for the Lewisian Gneiss Complex has been discussed by many authors (Park, 1995, Whitehouse and Bridgwater, 2001, Park, 2005, Kinny et al., 2005, Wheeler et al., 2010). Our new data (summarised in Table 8) contribute to the understanding of this evolution of the Lewisian, and hence of the Laurentian craton, through the Precambrian.

The TTG protoliths of the Lewisian Gneiss Complex originally formed within a number of crustal fragments or terranes at varying times within the Archaean (Kinny and Friend, 1997; Friend and Kinny, 2001; Kinny et al., 2005). Protolith ages within the Assynt terrane have previously been described as 3030-2960 Ma (Kinny et al., 2005) but our data also provide evidence for protoliths at c. 2843 Ma, an age more typically associated with the Rhiconich terrane. This suggests that the different terranes may all contain magmatic protoliths of a range of different ages.

Some of these terranes, most notably the Assynt terrane, underwent high-grade metamorphism during the Badcallian event, which has been variously linked with recognised dates for metamorphism at 2700-2800 Ma (Corfu et al., 1994; Whitehouse and Kemp, 2010) or 2490-2480 Ma (Kinny and Friend, 1997, Kinny et al., 2005). The Badcallian event produced granulite-facies metamorphic assemblages and crustal anatexis, but the driving causes of this event are not known. Subsequently, parts of the Lewisian Gneiss Complex were affected by the Inverian amphibolite-facies event with the formation of major shear zones (Evans, 1965), possibly at c.2480 Ma (Corfu et al., 1994; Zhu et al., 1997). Our data support a relatively high-temperature metamorphic event in the Laxford Shear Zone at c.

2480 Ma, which we link with the Inverian on the basis of relationships to Inverian structures. This event is recognised in both the Assynt and Gruinard terranes (Kinny et al., 2005), and it is likely that all the mainland Lewisian terranes to the north of Gairloch were assembled together at this time (Goodenough et al., 2010), with development of the Laxford Shear Zone. However, our data do not provide further constraints for the timing of the Badcallian event.

During the early part of the Palaeoproterozoic, the Lewisian Gneiss Complex largely lay within an extending continent, marked by the emplacement of the Scourie Dyke Swarm. By 1900 Ma, active margins existed along the edge of many continental fragments, creating a network of magmatic arcs which has been recognised across all the cratonic areas around the North Atlantic. Juvenile magmas formed in this setting were emplaced along the continental margin and within the Lewisian Gneiss Complex, where they followed the lines of weakness created by older terrane boundaries such as the Laxford Shear Zone. Subsequent collision of arc fragments led to localised high-temperature metamorphism in rocks associated with the South Harris Complex and Loch Maree Group (Love et al., 2010; Mason, 2012). Further north, many of the classic Laxfordian shear zones seen within the Assynt terrane are considered to have formed during this event, since they are cross-cut by undeformed granitoids emplaced at c. 1790-1770 Ma. This collisional event is considered to have been a part of the accretion of a major supercontinent, Columbia (or Nuna).

The subsequent metamorphic event or events, which began at c. 1790 Ma and continued to c. 1670 Ma, is recognised throughout the Lewisian Gneiss Complex and considered to represent the final assembly of all Lewisian terranes, particularly those in the southern part of the complex (Love et al., 2010). During this event, much of the Lewisian crust was buried and heated, with more fertile potassic gneisses such as those in the Rhiconich terrane melting to produce granites and pegmatites. The anhydrous granulite-facies gneisses of the Assynt terrane are relatively infertile (Watkins et al., 2007) and were not affected by melting.

Alteration and secondary growth of minerals such as monazite, titanite and rutile occurred in many lithologies within the Lewisian Gneiss Complex at this time. After c. 1670 Ma, the Lewisian Gneiss Complex became part of a stable craton, within a series of supercontinents.

Acknowledgements

This work is published with the permission of the Executive Director of the British Geological Survey. John Mendum and John Macdonald are thanked for their constructive comments on earlier versions of the paper. Constructive reviews by John Wheeler and Fernando Corfu, and editorial advice from Randy Parrish, were much appreciated, and have materially improved the paper. Dating work was funded through the BGS-NIGL funding scheme. This is a contribution to IGCP-SIDA Project 599 (The Changing Early Earth).

References

Beach, A., Coward, M. P.,Graham, R. H., 1974. An interpretation of the structural evolution of the Laxford front. *Scottish Journal of Geology* 9**,** 297-308.

Black, L. P.,Gulson, B. L., 1978. The age of the Mud Tank carbonatite, Strangways Range, Northern Territory. *BMR Journal of Australian Geology and Geophysics* 3**,** 227-232.

Bowes, D. R., 1962. Untitled discussion. *Proceedings of the Geological Society of London* 1594**,** 28-30.

Bowes, D. R. 1968. An orogenic interpretation of the Lewisian of Scotland. 23rd International Geological Congress. 225-236.

Chapman, H. J.,Moorbath, S., 1977. Lead isotope measurements from the oldest recognised Lewisian gneisses of north-west Scotland. *Nature* 268**,** 41-42.

Cohen, A. S., O'Nions, R. K.,O'Hara, M. J., 1991. Chronology and mechanism of depletion in Lewisian granulites *Contributions to Mineralogy and Petrology* 106**,** 142-153.

Corfu, F., Heaman, L. M.,Rogers, G., 1994. Polymetamorphic evolution of the Lewisian complex, NW Scotland, as recorded by U-Pb isotopic compositions of zircon, titanite and rutile. *Contributions to Mineralogy and Petrology* 117**,** 215-228.

Coward, M. P., 1990. Shear zones at the Laxford front, NW Scotland and their significance in the interpretation of lower crustal structure. *Journal of the Geological Society of London* 147**,** 279-286.

Daly, J. S., Balagansky, V. V., Timmerman, M. J.,Whitehouse, M. J., 2006. The Lapland-Kola orogen: Palaeoproterozoic collision and accretion of the northern Fennoscandian lithosphere. *Geological Society of London Memoir* 32**,** 579-598.

Daly, J. S., Muir, R. J.,Cliff, R. A., 1991. A precise U-Pb zircon age for the Inishtrahull syenitic gneiss, County Donegal, Ireland. *Journal of the Geological Society of London* 148**,** 639-642.

Davies, F. B., 1974. A layered basic complex in the Lewisian, south of Loch Laxford, Sutherland. *Journal of the Geological Society of London* 130**,** 279-284.

Davies, F. B., 1976. Early Scourian structures in the Scourie-Laxford region and their bearing on the evolution of the Laxford Front. *Journal of the Geological Society of London* 132**,** 543-554.

Evans, C. R., 1965. Geochronology of the Lewisian basement near Lochinver, Sutherland. *Nature* 207**,** 54-56.

Evans, C. R.,Lambert, R. S. J., 1974. The Lewisian of Lochinver, Sutherland: the type area for the Inverian metamorphism. *Journal of the Geological Society of London* 130**,** 125-150.

Friend, C. R. L.,Kinny, P. D., 1995. New evidence for protolith ages of Lewisian granulites, northwest Scotland. *Geology* 23**,** 1027-1030.

Friend, C. R. L.,Kinny, P. D., 2001. A reappraisal of the Lewisian Gneiss Complex: geochronological evidence for its tectonic assembly from disparate terranes in the Proterozoic. *Contributions to Mineralogy and Petrology* 142**,** 198-218.

Garde, A. A., Chadwick, B., Grocott, J., Hamilton, M. A., McCaffrey, K. J.,Swager, C. P., 2002b. Mid-crustal partitioning and attachment during oblique convergence in an arc system, Palaeoproterozoic Ketilidian orogen, southern Greenland *Journal of the Geological Society of London* 159**,** 247-261.

Garde, A. A., Hamilton, M. A., Chadwick, B., Grocott, J.,McCaffrey, K. J., 2002a. The Ketilidian orogen of South Greenland: geochronology, tectonics, magmatism, and fore-arc accretion during Palaeoproterozoic oblique convergence *Canadian Journal of Earth Sciences* 39**,** 765-793.

Giletti, B. J., Moorbath, S.,Lambert, R. S. J., 1961. A geochronological study of the metamorphic complexes of the Scottish Highlands. *Quarterly Journal of the Geological Society of London* 117**,** 233-264.

Goodenough, K. M., Park, R. G., Krabbendam, M., Myers, J. S., Wheeler, J., Loughlin, S., Crowley, Q., L, F. C. R., Beach, A., Kinny, P. D.,Graham, R., 2010. The Laxford Shear Zone: an end-Archaean terrane boundary? *In:* Law, R., Butler, R. W. H., Holdsworth, R. E., Krabbendam, M.,Strachan, R. (eds.), *Continental Tectonics and Mountain Building.*Geological Society Special Publication 335. London: The Geological Society.

Hamilton, P. J., Evensen, N. M., O'Nions, R. K.,Tarney, J., 1979. Sm-Nd systematics of Lewisian gneisses: implications for the origin of granulites. *Nature* 277**,** 25-28.

Heaman, L.,Tarney, J., 1989. U-Pb baddeleyite ages for the Scourie dyke swarm, Scotland: evidence for two distinct intrusion events. *Nature, London* 340**,** 705-708.

Holmes, A., Shillibeer, H. A.,Wilson, J. T., 1955. Potassium-Argon Ages of Some Lewisian and Fennoscandian Pegmatites. *Nature* 176**,** 390-392.

Jackson, S. E., Pearson, N. J., Griffin, W. L.,Belousova, E., 2004. The application of laser ablation inductively coupled plasma mass spectrometry to in-situ U–Pb zircon geochronology. *Chemical Geology* 211**,** 47-69.

Johnson, T. E., Fischer, S., White, R. W., Brown, M.,Rollinson, H. R., 2012. Archaean Intracrustal Differentiation from Partial Melting of Metagabbro - Field and Geochemical Evidence from the Central Region of the Lewisian Complex, NW Scotland. *Journal of Petrology* 53**,** 2115-2138.

Kalsbeek, F.,Nutman, A. P., 1996. Anatomy of the Early Proterozoic Nagssugtoqidian orogen, West Greenland, explored by reconnaissance SHRIMP U-Pb zircon dating. *Geology* 24**,** 515-518.

Kinny, P.,Friend, C., 1997. U-Pb isotopic evidence for the accretion of different crustal blocks to form the Lewisian Complex of Northwest Scotland. *Contributions to Minerology and Petrology*.

Kinny, P. D., Friend, C. R. L.,J, L. G., 2005. Proposal for a terrane-based nomenclature for the Lewisian Complex of NW Scotland. *Journal of the Geological Society of London* 162**,** 175-186.

Lahtinen, R., Korja, A., Nironen, M.,Heikkinen, P., 2009. Palaeoproterozoic accretionary processes in Fennoscandia. *In:* Cawood, P. A.,Kroner, A. (eds.), *Earth Accretionary Systems in Space and Time.*Geological Society Special Publication 318. London: Geological Society, London.

Lambert, R. S. J.,Holland, J. G., 1972. A geochronological study of the Lewisian from Loch Laxford to Durness, Sutherland, N W Scotland. *Journal of the Geological Society of London* 128**,** 3-19.

Love, G. J., Friend, C. R. L.,Kinny, P. D., 2010. Palaeoproterozoic terrane assembly in the Lewisian Gneiss Complex on the Scottish mainland, south of Gruinard Bay: SHRIMP U–Pb zircon evidence. *Precambrian Research* 183**,** 89-111.

Love, G. J., Kinny, P.,Friend, C. R. L., 2004. Timing of magmatism and metamorphism in the Gruinard Bay area of the Lewisian Gneiss Complex: comparisons with the Assynt Terrane and implications for terrane accretion *Contributions to Mineralogy and Petrology* 146**,** 620-636.

Ludwig, K. R., 1980. Calculation of uncertainties of U-Pb isotope Data. *Earth and Planetary Science Letters* 46**,** 212-220.

Ludwig, K. R., 1993. Pbdat: a computer program for processing Pb-U-Th isotope data. *United States Geological Survey, Open file reports.* 88-542**,** 1-34.

Ludwig, K. R., 2003. Isoplot 3.00: A geochronological toolkit for Microsoft Excel. *Berkeley Geochronology Centre Special Publication* 4**,** 0-71.

Marcantonio, F., Dickin, A. P., McNutt, R. H.,Heaman, L. M., 1988. A 1,800-million-year-old Proterozoic gneiss terrane in Islay with implications for the crustal structure and evolution of Britain. *Nature* 335**,** 62-64.

Mason, A. J., 2012. Major early thrusting as a control on the Palaeoproterozoic evolution of the Lewisian Complex: evidence from the Outer Hebrides, NW Scotland. *Journal of the Geological Society of London* 169**,** 201-212.

Mason, A. J.,Brewer, T. S., 2005. A re-evaluation of a Laxfordian terrane boundary in the Lewisian Complex of South Harris, NW Scotland. *Journal of the Geological Society of London* 162**,** 401-408.

Mason, A. J., Parrish, R. R.,Brewer, T. S., 2004. U–Pb geochronology of Lewisian orthogneisses in the Outer Hebrides, Scotland: implications for the tectonic setting and correlation of the South Harris Complex *Journal of the Geological Society of London* 2004**,** 45-54.

Mattinson, J. M., 2005. Zircon U-Pb chemical abrasion ("CA-TIMS") method: Combined annealing and multi-step partial dissolution analysis for improved precision and accuracy of zircon ages. *Chemical Geology* 220**,** 47-66.

McAteer, C. A., Daly, J. S., Flowerdew, M. J., Connelly, J. N., Housh, T. B.,Whitehouse, M. J., 2010. Detrital zircon, detrital titanite and igneous clast U–Pb geochronology and basement–cover relationships of the Colonsay Group, SW Scotland: Laurentian provenance and correlation with the Neoproterozoic Dalradian Supergroup. *Precambrian Research* 181**,** 21-42.

Moorbath, S., Welke, H.,Gale, N., 1969. The significance of lead isotope studies in ancient, high-grade metamorphic basement complexes, as exemplified by the Lewisian rocks of Northwest Scotland *Earth and Planetary Science Letters* 6**,** 245-256.

Mundil, R., Ludwig, K. R., Metcalfe, I.,Renne, P. R., 2004. Age and timing of the Permian mass extinctions: U-Pb dating of closed-system zircons *Science* 305**,** 1760-1763.

Nutman, A. P., Kalsbeek, F.,Friend, C. R. L., 2008. The Nagssugtoqidian orogen in South-East Greenland: Evidence for Paleoproterozoic collision and plate assembly. *American Journal of Science* 308**,** 529-572.

Park, R. G., 1970. Observations on Lewisian chronology. *Scottish Journal of Geology* 6**,** 379-399.

Park, R. G., 1995. Palaeoproterozoic Laurentia-Baltica relationships: a view from the Lewisian. *In:* Coward, M. P.,Ries, A. C. (eds.), *Early Precambrian Processes.*Geological Society Special Publication 95. London: The Geological Society.

Park, R. G., 2005. The Lewisian terrane model: a review. *Scottish Journal of Geology* 41**,** 105-118.

Park, R. G.,Tarney, J., 1987. The Lewisian complex: a typical Precambrian high-grade terrain? *In:* Park, R. G.,Tarney, J. (eds.), *Evolution of the Lewisian and Comparable Precambrian High Grade Terrains.*27. London: Geological Society of London Special Publication.

Park, R. G., Tarney, J.,Connelly, J. N., 2001. The Loch Maree Group: Palaeoproterozoic subduction–accretion complex in the Lewisian of NW Scotland. *Precambrian Research* 105**,** 205-226.

Peach, B. N., Horne, J., Gunn, W., Clough, C. T., Hinxman, L. W.,Teall, J. J. H., 1907. *The geological structure of the North-West Highlands of Scotland*, Memoir of the Geological Survey of Great Britain.

Pidgeon, R. T.,Bowes, D. R., 1972. Zircon U–Pb ages of granulites from the Central Region of the Lewisian, northwestern Scotland. *Geological Magazine* 109**,** 247-258.

Rogers, J. J. W.,Santosh, M., 2002. Configuration of Columbia, a Mesoproterozoic Supercontinent. *Gondwana Research* 5**,** 5-22.

Rollinson, H. R.,Windley, B. F., 1980. Geochemistry and origin of an Archaean granulite grade tonalite-trondhjemite-granite suite from Scourie, NW Scotland. *Contributions to Mineralogy and Petrology* 72**,** 265-281.

Scott, D. J., 1998. An overview of the U-Pb geochronology of the Paleoproterozoic Torngat Orogen, Northeastern Canada. *Precambrian Research* 91**,** 91-107.

St-Onge, M. R., van Gool, J. A. M., Garde, A. A.,Scott, D. J., 2009. Correlation of Archaean and Palaeoproterozoic units between northeastern Canada and western Greenland: constraining the pre-collisional upper plate accretionary history of the Trans-Hudson orogen. *In:* Cawood, P. A.,Kroner, A. (eds.), *Earth Accretionary Systems in Space and Time.*Geological Society Special Publication 318. London: The Geological Society, London.

Stacey, J. S.,Kramer, J. D., 1975. Approximation of terrestrial lead isotope evolution by a two stage model. *Earth and Planetary Science Letters* 26**,** 207-221.

Sutton, J.,Watson, J. V., 1951. The pre-Torridonian metamorphic history of the Loch Torridon and Scourie areas in the northwest Highlands, and its bearing on the chronological classification of the Lewisian. *Quarterly Journal of the Geological Society of London* 106**,** 241-307.

Tarney, J.,Weaver, B. L., 1987. Geochemistry of the Scourian complex: petrogenesis and tectonic models. *In:* Park, R. G.,Tarney, J. (eds.), *Evolution of the Lewisian and Comparable Precambrian High Grade Terrains.*Geological Society of London Special Publication 27. London: Geological Society of London.

Thomas, R. J., Jacobs, J., Horstwood, M. S. A., Ueda, K., Bingen, B.,Matola, R., 2010. The Mecubúri and Alto Benfica Groups, NE Mozambique: aids to unravelling ca.1 Ga and 0.5 Ga events in the East African Orogen. *Precambrian Research* 178**,** 72-90.

van Gool, J. A. M., Connelly, J. N., Marker, M.,Mengel, F. C., 2002. The Nagssugtoqidian Orogen of West Greenland: tectonic evolution and regional correlations from a West Greenland perspective *Canadian Journal of Earth Sciences* 39**,** 665-686.

van Kranendonk, M. J., St-Onge, M. R.,Henderson, J. R., 1993. Paleoproterozoic tectonic assembly of Northeast Laurentia through multiple indentations. *Precambrian Research* 63**,** 325-347.

Watkins, J. M., Clemens, J. D.,Treloar, P. J., 2007. Archean TTGs as sources of younger granitic magmas: melting of sodic metatonalites at 0.6-1.2 GPa. *Contributions to Mineralogy and Petrology* 154**,** 91-110.

Wheeler, J., Park, R. G., Rollinson, H. R.,Beach, A., 2010. The Lewisian Complex: insights into deep crustal evolution. *In:* Law, R., Butler, R. W. H., Holdsworth, R. E., Krabbendam, M.,Strachan, R. (eds.), *Continental Tectonics and Mountain Building: the Legacy of Peach and Horne.*Geological Society Special Publication 335. London: The Geological Society.

Whitehouse, M. J., 1989. Sm-Nd evidence for diachronous crustal accretion in the Lewisian complex of northwest Scotland. *Tectonophysics* 161**,** 245-256.

Whitehouse, M. J., 1990. An early-Proterozoic age for the Ness anorthosite, Lewis, Outer Hebrides. *Scottish Journal of Geology* 26**,** 131-136.

Whitehouse, M. J.,Bridgwater, D., 2001. Geochronological constraints on Paleoproterozoic crustal evolution and regional correlations of the northern Outer Hebridean Lewisian complex, Scotland. *Precambrian Research* 105**,** 227-245.

Whitehouse, M. J.,Kemp, A. I. S., 2010. On the difficulty of assigning crustal residence, magmatic protolith and metamorphic ages to Lewisian granulites: constraints from combined in situ U-Pb and Lu-Hf isotopes. *In:* Law, R., Butler, R. W. H., Holdsworth, R. E., Krabbendam, M.,Strachan, R. (eds.), *Continental Tectonics and Mountain Building: the Legacy of Peach and Horne.*Geological Society Special Publication 335. London: Geological Society of London.

Whitehouse, M. J.,Moorbath, S., 1986. Pb−Pb systematics of Lewisian gneisses—implications for crustal differentiation. *Nature* 319**,** 488-489.
Zhao, G., Sun, M., Wilde, S. A.,Li, S., 2004. A Paleo-Mesoproterozoic supercontinent: assembly, growth and breakup. *Earth Science Reviews* 67**,** 91-123.
Zhu, X. K., O'Nions, R. K., Belshaw, N. S.,Gibb, A. J., 1997. Lewisian crustal history from in situ SIMS mineral chronometry and related metamorphic textures. *Chemical Geology* 136**,** 205-218.
Zirkler, A., Johnson, T. E., White, R. W.,Zack, T., 2012. Polymetamorphism in the mainland Lewisian complex, NW Scotland - phase equilibria and geochronological constraints from the Cnoc an t'Sidhean suite. *Journal of Metamorphic Geology* 30**,** 865-885.

Figure captions

1. Generalised map of the Lewisian Gneiss Complex in Northwest Scotland, showing the main structural features, after Kinny et al. (2005) and Wheeler et al. (2010).
2. Simplified geological map of the Laxford Shear Zone, after Goodenough et al. (2010). Sample localities: 1, Badnabay; 2, Tarbet; 3, Ben Stack; 4, Rhiconich
3. a) Photograph of the Tarbet locality, showing granite sheets that have been tightly folded by Inverian deformation; sample LX11 was collected from one of these granite sheets. c. 80 cm sledgehammer for scale. b) Photograph of the Rhiconich locality, showing anastomosing, undeformed granite sheets; sample LX7 was collected from one of these.
4. Representative CL images of zircon grains from the dated samples LX1, LX2, LX6, LX7, and LX11.
5. Concordia plots for samples from Badnabay and Tarbet. a) U-Pb zircon ID-TIMS data for sample LX1; b) U-Pb zircon LA-ICPMS data for sample LX1; c) U-Pb zircon concordia diagram for sample LX2; d) U-Pb zircon concordia diagram for sample LX11. All data-point error ellipses are 2σ.
6. Concordia plots for samples from Ben Stack and Rhiconich. a) U-Pb concordia diagram for all data from sample LX6, b) probability plot showing ^{207}Pb/^{206}Pb age

for sample LX6, c) U-Pb concordia diagram of c. 1880 Ma population from LX6; d) Tera Wasserburg diagram for sample LX6 titanites; e) U-Pb zircon concordia diagram for all data from sample LX7; f) U-Pb zircon concordia diagram for c. 1790 Ma cluster from sample LX7. All data-point error ellipses are 2σ.

Tables (may be published as supplementary data if necessary)

1. LA-ICPMS U-Pb data for zircon from LX1
2. TIMS U-Pb data for zircon from LX1
3. LA-ICPMS data for zircon from LX2
4. LA-ICPMS data for zircon from LX11
5. LA-ICPMS data for zircon from LX6
6. LA-ICPMS data for titanite from LX6
7. LA-ICPMS data for zircon from LX7
8. Summary of the dates for the Lewisian Gneiss Complex presented in this paper.

Analysis	(mV) ^{206}Pb	^{207}Pb	^{238}U	Concentrations (ppm) Pb	U*	†Ratios $^{207}Pb/^{206}Pb$	±1s %	$^{206}Pb/^{238}U$	±1s %	$^{207}Pb/^{235}U$	±1s %	Rho	Ages (Ma) $^{207}Pb/^{206}Pb$	±2s abs	$^{206}Pb/^{238}U$	±2s abs	$^{207}Pb/^{235}U$	±2s abs	§% disc
LX-1_Z1_1	0.27	0.04	0.68	2	4	0.1751	2.0	0.5036	2.7	12.1552	3.4	0.80	2607	34	2629	173	2616	608	-1
LX-1_Z1_2	0.59	0.10	1.38	5	9	0.1867	1.0	0.5553	1.8	14.2974	2.1	0.86	2714	17	2847	128	2770	475	-5
LX-1_Z1_3	1.34	0.25	2.81	10	18	0.2050	0.7	0.6037	1.1	17.0669	1.3	0.83	2867	12	3045	82	2939	369	-6
LX-1_Z1_4	1.52	0.24	3.63	12	24	0.1789	0.7	0.5240	1.0	12.9268	1.2	0.83	2643	11	2716	69	2674	281	-3
LX-1_Z1_5	1.06	0.19	2.41	8	16	0.2003	0.7	0.5485	1.1	15.1487	1.3	0.83	2829	12	2819	75	2825	334	0
LX-1_Z2_1	8.67	0.85	33.51	67	217	0.1100	0.5	0.3298	0.9	5.0033	1.0	0.87	1800	9	1838	37	1820	97	-2
LX-1_Z2_2	11.61	1.14	46.06	90	298	0.1105	0.1	0.3264	0.9	4.9724	0.9	0.99	1807	2	1821	36	1815	84	-1
LX-1_Z2_3	4.16	0.41	16.15	32	104	0.1113	0.3	0.3179	0.9	4.8801	0.9	0.94	1822	6	1779	36	1799	90	2
LX-1_Z2_4	4.45	0.44	17.06	35	110	0.1107	0.5	0.3185	0.9	4.8619	1.0	0.87	1811	9	1782	37	1796	96	2
LX-1_Z2_5	12.89	1.76	37.21	100	241	0.1531	1.0	0.4210	1.1	8.8885	1.4	0.74	2381	17	2265	58	2327	233	5
LX-1_Z2_6	6.60	0.65	24.40	51	158	0.1109	0.5	0.3342	0.9	5.1106	1.1	0.88	1815	9	1859	40	1838	105	-2
LX-1_Z3_1	3.89	0.45	13.32	30	86	0.1305	0.3	0.3700	1.0	6.6585	1.0	0.95	2105	6	2029	46	2067	130	4
LX-1_Z3_2	3.39	0.36	12.45	26	81	0.1202	0.4	0.3485	0.9	5.7738	1.0	0.91	1959	7	1927	42	1942	115	2
LX-1_Z3_3	4.48	0.54	14.76	35	96	0.1350	0.3	0.3879	1.0	7.2232	1.0	0.95	2165	5	2113	49	2139	140	2
LX-1_Z4_1	12.14	1.86	32.52	94	210	0.1725	0.3	0.4745	1.1	11.2836	1.1	0.96	2582	5	2503	64	2547	224	3
LX-1_Z5_1	4.27	0.41	16.81	33	109	0.1079	0.3	0.3263	1.0	4.8532	1.0	0.96	1764	6	1821	41	1794	97	-3
LX-1_Z5_2	3.47	0.34	13.20	27	85	0.1106	0.4	0.3203	0.8	4.8831	0.9	0.92	1809	7	1791	35	1799	88	1
LX-1_Z5_3	1.73	0.17	6.46	13	42	0.1103	0.6	0.3279	0.9	4.9860	1.1	0.84	1804	11	1828	39	1817	105	-1
LX-1_Z5_4	1.09	0.11	3.95	8	26	0.1110	0.5	0.3400	1.1	5.2026	1.2	0.91	1816	9	1886	47	1853	119	-4
LX-1_Z6_1	4.50	0.44	17.58	35	114	0.1088	0.3	0.3301	1.0	4.9495	1.0	0.96	1779	6	1839	42	1811	100	-3
LX-1_Z6_2	2.91	0.28	11.17	23	72	0.1087	0.4	0.3130	0.8	4.6917	0.9	0.90	1778	7	1755	33	1766	83	1
LX-1_Z6_3	1.70	0.17	6.22	13	40	0.1097	0.5	0.3322	0.8	5.0252	1.0	0.86	1795	9	1849	36	1824	96	-3
LX-1_Z7_1	13.79	2.11	37.81	107	245	0.1730	0.1	0.4724	1.0	11.2682	1.0	0.99	2587	2	2494	61	2546	208	4
LX-1_Z8_1	4.93	0.48	19.23	38	124	0.1083	0.3	0.3291	0.9	4.9134	0.9	0.96	1770	5	1834	37	1805	88	-4
LX-1_Z8_2	1.98	0.19	7.36	15	48	0.1108	0.5	0.3247	0.8	4.9600	1.0	0.86	1813	9	1812	35	1813	93	0
LX-1_Z8_3	1.23	0.12	4.41	10	29	0.1106	0.5	0.3348	1.0	5.1036	1.1	0.89	1808	9	1862	42	1837	108	-3
LX-1_Z8_4	1.80	0.18	6.74	14	44	0.1100	0.6	0.3246	0.8	4.9221	1.0	0.81	1799	11	1812	34	1806	97	-1
LX-1_Z9_1	15.72	2.55	39.87	122	258	0.1820	0.2	0.5032	0.9	12.6310	1.0	0.97	2672	4	2628	61	2653	223	2
LX-1_Z10_1	7.06	0.68	28.12	55	182	0.1084	0.2	0.3240	0.8	4.8438	0.9	0.97	1773	4	1809	35	1793	82	-2
LX-1_Z10_2	7.02	0.68	27.71	54	179	0.1078	0.2	0.3270	0.9	4.8619	0.9	0.97	1763	4	1824	37	1796	86	-3
LX-1_Z10_3	4.22	0.41	14.74	33	95	0.1091	0.3	0.3357	0.8	5.0490	0.9	0.94	1784	6	1866	36	1828	88	-5
LX-1_Z10_4	4.33	0.42	16.12	34	104	0.1094	0.5	0.3211	0.8	4.8432	1.0	0.86	1789	9	1795	35	1792	92	0
LX-1_Z10_5	4.35	0.43	16.27	34	105	0.1098	0.3	0.3205	0.8	4.8533	0.9	0.94	1797	5	1792	35	1794	84	0
LX-1_Z10_6	4.15	0.40	14.91	32	96	0.1091	0.4	0.3334	1.0	5.0139	1.1	0.94	1784	6	1855	43	1822	104	-4
LX-1_Z10_7	4.27	0.42	16.06	33	104	0.1110	0.3	0.3197	0.9	4.8922	1.0	0.96	1816	5	1788	39	1801	93	2

*Accuracy of U concentration is *c* .20%

†Isotope ratios are not common Pb corrected

§% Discordance is measured as $^{206}Pb/^{238}U$ age relative to $^{207}Pb/^{206}Pb$ age

	weight (μg)	U(ppm)	Pb(ppm)†	Pb (pg)‡	Th/U	Isotopic ratios								Ages (Ma)					
						$^{206}Pb/^{204}Pb$§	$^{207}Pb/^{206}Pb$¶	2σ (%)	$^{206}Pb/^{238}U$¶	2σ (%)	$^{207}Pb/^{235}U$¶	2σ (%)	Rho⌐	$^{207}Pb/^{206}Pb$	2σ (Ma)	$^{206}Pb/^{238}U$	2σ (Ma)	$^{207}Pb/^{235}U$	2σ (Ma)
LX-1																			
Z1	0.1	684.6	249.6	1.3	0.8	1081.1	0.10843	0.12	0.31644	0.19	4.73093	0.23	0.85	1773.3	2.2	1772.3	3.3	1772.7	4.0
Z2	0.2	442.3	148.8	1.7	0.4	1044.7	0.10835	0.12	0.31572	0.27	4.71683	0.30	0.91	1771.9	2.2	1768.8	4.7	1770.2	5.2
Z3	0.5	470.2	192.2	2.6	1.3	1664.3	0.10810	0.16	0.30922	0.18	4.60888	0.24	0.77	1767.6	2.8	1736.9	3.2	1750.9	4.3
Z4	0.2	510.8	206.0	2.2	1.1	919.4	0.10846	0.09	0.31582	0.23	4.72293	0.25	0.93	1773.7	1.7	1769.3	4.1	1771.3	4.5
Z5	0.3	96.4	43.7	2.1	0.9	303.9	0.12695	0.39	0.34218	0.73	5.98938	0.85	0.89	2056.1	6.9	1897.2	13.8	1974.3	16.7

*Samples not being subjected to ion-exchange procedures
†Radiogenic lead corrected for mass fractionation, laboratory Pb, spike and initial common Pb
‡Total common Pb
§$^{206}Pb/^{204}Pb$ is a measured ratio corrected for mass fractionation and common lead in the $^{205}Pb/^{235}U$ spike
¶Corrected for mass fractionation, laboratory Pb & U spike and initial common Pb
⌐Error correlation coefficient calculated using isoplot (Ludwig, 2003)

	(mV)			Concentrations (ppm)		†Ratios							Ages (Ma)						§% disc
Analysis	^{206}Pb	^{207}Pb	^{238}U	Pb	U*	^{207}Pb/^{206}Pb	±1s %	^{206}Pb/^{238}U	±1s %	^{207}Pb/^{235}U	±1s %	Rho	^{207}Pb/^{206}Pb	±2s abs	^{206}Pb/^{238}U	±2s abs	^{207}Pb/^{235}U	±2s abs	
LX-2_Z1_1	9.39	1.57	22.13	73	143	0.1874	0.2	0.5122	0.9	13.2330	1.0	0.97	2719	4	2666	62	2696	232	2
LX-2_Z1_2	6.87	1.00	17.74	53	115	0.1628	0.1	0.4681	1.0	10.5088	1.0	0.99	2485	2	2475	60	2481	196	0
LX-2_Z1_3	3.82	0.55	9.89	30	64	0.1618	0.2	0.4749	0.9	10.5949	0.9	0.97	2475	4	2505	55	2488	184	-1
LX-2_Z2_1	12.52	2.10	29.05	97	188	0.1898	0.2	0.5256	1.1	13.7556	1.1	0.98	2740	4	2723	73	2733	270	1
LX-2_Z2_2	12.69	2.13	29.44	98	191	0.1886	0.1	0.5289	0.9	13.7523	0.9	0.99	2730	2	2737	63	2733	234	0
LX-2_Z2_3	17.25	2.88	40.33	134	261	0.1869	0.5	0.5231	1.0	13.4821	1.2	0.90	2715	8	2712	70	2714	275	0
LX-2_Z3_1	9.91	1.62	23.63	77	153	0.1834	0.3	0.5163	1.0	13.0584	1.1	0.97	2684	5	2683	69	2684	252	0
LX-2_Z3_2	8.97	1.56	19.96	70	129	0.1950	0.3	0.5432	1.0	14.6024	1.0	0.94	2784	6	2797	67	2790	263	0
LX-2_Z3_3	8.34	1.41	19.34	65	125	0.1898	0.5	0.5320	1.1	13.9238	1.2	0.91	2741	8	2750	75	2745	293	0
LX-2_Z4_1	12.26	1.87	29.42	95	190	0.1712	0.4	0.5137	1.1	12.1276	1.1	0.95	2570	6	2672	70	2614	243	-4
LX2_Z5_1	8.77	1.37	24.86	84	173	0.1730	0.2	0.4953	1.2	11.8118	1.2	0.99	2587	3	2594	76	2590	254	0
LX2_Z5_2	8.71	1.35	24.95	83	173	0.1716	0.2	0.4970	1.2	11.7593	1.2	0.99	2573	3	2601	76	2585	253	-1
LX2_Z5_3	8.76	1.32	25.55	84	177	0.1668	0.3	0.4830	1.2	11.1089	1.2	0.98	2526	4	2540	72	2532	238	-1
LX2_Z5_4	8.96	1.43	25.32	86	176	0.1753	0.4	0.5016	1.1	12.1245	1.2	0.95	2609	6	2621	73	2614	258	0
LX2_Z5_6	3.39	0.50	10.30	32	72	0.1629	0.3	0.4800	1.2	10.7818	1.2	0.96	2486	6	2527	73	2505	238	-2
LX2_Z6_1	5.30	0.88	14.25	51	99	0.1832	0.2	0.5276	1.2	13.3305	1.2	0.99	2682	3	2731	81	2703	285	-2
LX2_Z6_2	7.39	1.23	19.90	71	138	0.1839	0.5	0.5264	1.2	13.3496	1.3	0.93	2689	8	2726	84	2705	310	-1
LX2_Z7_1	6.57	1.04	18.42	63	128	0.1740	0.3	0.5066	1.2	12.1575	1.3	0.98	2597	5	2642	80	2617	272	-2
LX2_Z7_2	6.87	1.08	19.34	66	134	0.1729	0.3	0.5054	1.2	12.0489	1.2	0.97	2586	5	2637	75	2608	257	-2
LX2_Z8_1	2.28	0.40	5.85	22	41	0.1922	0.5	0.5485	1.3	14.5343	1.4	0.92	2761	9	2819	90	2785	343	-2
LX-2_Z9_1	6.66	1.01	19.54	64	136	0.1679	0.2	0.4861	1.3	11.2513	1.3	0.99	2537	4	2554	80	2544	262	-1
LX-2_Z9_2	9.44	1.58	25.69	90	178	0.1840	0.5	0.5216	1.4	13.2324	1.5	0.93	2689	9	2706	95	2696	345	-1
LX-2_Z9_3	10.33	1.73	28.01	99	195	0.1855	0.3	0.5219	1.2	13.3443	1.3	0.97	2702	5	2707	83	2704	300	0
LX-2_Z9_4	2.92	0.45	8.81	28	61	0.1685	0.4	0.4793	1.2	11.1364	1.2	0.95	2543	6	2524	71	2535	242	1
LX-2_Z9_5	2.86	0.44	8.74	27	61	0.1681	0.5	0.4797	1.2	11.1212	1.3	0.92	2539	8	2526	73	2533	255	1
LX-2_Z10_1	7.62	1.23	21.34	73	148	0.1788	0.2	0.5044	1.2	12.4378	1.2	0.99	2642	3	2633	78	2638	271	0
LX-2_Z10_2	8.47	1.41	23.22	81	161	0.1842	0.8	0.5161	1.3	13.1051	1.5	0.85	2691	13	2683	83	2687	331	0
LX-2_Z10_3	12.48	1.86	37.34	119	259	0.1646	0.2	0.4745	1.2	10.7704	1.2	0.99	2504	3	2503	72	2504	234	0
LX-2_Z11_1	6.34	1.06	17.44	61	121	0.1840	0.3	0.5178	1.2	13.1345	1.2	0.98	2689	4	2690	81	2689	287	0
LX-2_Z11_2	13.82	2.29	38.70	132	269	0.1834	0.2	0.5033	1.3	12.7294	1.3	0.99	2684	4	2628	85	2660	298	2
LX-2_Z11_3	5.28	0.88	14.59	50	101	0.1850	0.3	0.5107	1.3	13.0292	1.3	0.98	2699	4	2660	82	2682	294	1
LX-2_Z12_1	4.53	0.75	12.24	43	85	0.1840	0.4	0.5252	1.1	13.3250	1.2	0.93	2689	7	2721	74	2703	276	-1
LX-2_Z13_1	4.78	0.77	13.55	46	94	0.1771	0.5	0.5107	1.2	12.4723	1.3	0.93	2626	8	2660	80	2641	290	-1
LX-2_Z13_2	5.95	0.91	17.72	57	123	0.1686	0.2	0.4832	1.2	11.2305	1.2	0.99	2543	3	2541	75	2542	247	0
LX-2_Z14_1	5.47	0.88	15.94	52	111	0.1773	0.3	0.4989	1.3	12.1976	1.3	0.98	2628	4	2609	83	2620	283	1
LX-2_Z14_2	5.82	0.93	16.99	56	118	0.1750	0.5	0.4965	1.1	11.9796	1.2	0.91	2606	8	2599	71	2603	261	0
LX-2_Z14_3	6.02	1.03	16.53	58	115	0.1894	0.2	0.5326	1.2	13.9072	1.2	0.99	2737	3	2752	80	2743	291	-1
LX-2_Z16_3	13.94	2.15	42.85	133	298	0.1703	0.3	0.4678	1.4	10.9819	1.4	0.98	2560	4	2474	83	2522	274	3
LX-2_Z17_1	5.26	0.82	15.41	50	107	0.1725	0.3	0.4977	1.1	11.8362	1.2	0.97	2582	5	2604	72	2592	248	-1
LX-2_Z18_1	4.75	0.76	13.75	45	96	0.1759	0.2	0.5040	1.1	12.2250	1.2	0.98	2615	4	2631	73	2622	253	-1
LX-2_Z18_2	3.93	0.68	10.87	38	76	0.1909	0.7	0.5296	1.1	13.9365	1.3	0.85	2750	12	2740	76	2745	319	0
LX-2_Z19_1	6.10	0.91	18.60	58	129	0.1644	0.2	0.4790	1.1	10.8579	1.2	0.98	2502	4	2523	70	2511	228	-1
LX-2_Z19_2	6.60	1.11	18.92	63	131	0.1851	0.5	0.5046	1.1	12.8818	1.2	0.93	2699	8	2634	72	2671	275	2
LX-2_Z19_4	2.32	0.35	6.99	22	49	0.1692	0.4	0.4949	1.3	11.5441	1.4	0.97	2549	6	2592	85	2568	283	-2
LX-2_Z20_1	8.26	1.28	25.12	79	175	0.1704	0.2	0.4757	1.2	11.1758	1.2	0.99	2562	3	2508	71	2538	237	2
LX-2_Z20_2	8.50	1.47	23.68	81	165	0.1913	0.5	0.5271	1.2	13.9036	1.3	0.92	2754	8	2729	79	2743	309	1
LX-2_Z20_3	2.73	0.40	8.62	26	60	0.1631	0.3	0.4694	1.1	10.5548	1.2	0.96	2488	6	2481	68	2485	224	0
LX-2_Z20_4	2.60	0.40	7.69	25	53	0.1707	0.3	0.4964	1.1	11.6820	1.2	0.96	2564	6	2598	73	2579	249	-1
LX-2_Z21_1	10.58	1.73	30.80	101	214	0.1806	0.2	0.5010	1.2	12.4762	1.2	0.99	2658	3	2618	75	2641	263	2
LX-2_Z21_2	11.15	1.90	31.10	107	216	0.1872	0.5	0.5180	1.1	13.3726	1.3	0.92	2718	8	2691	76	2706	293	1
LX-2_Z22_1	8.90	1.48	25.39	85	176	0.1837	0.5	0.5086	1.2	12.8858	1.3	0.93	2687	8	2651	81	2671	301	1
LX-2_Z22_2	6.95	1.15	19.08	66	133	0.1833	0.4	0.5246	1.3	13.2608	1.3	0.96	2683	6	2719	87	2698	310	-1
LX-2_Z23_1	8.84	1.46	24.57	85	171	0.1835	0.5	0.5247	1.4	13.2777	1.5	0.94	2685	8	2719	96	2700	345	-1
LX-2_Z23_2	8.75	1.44	24.40	84	169	0.1820	0.5	0.5214	1.2	13.0811	1.3	0.92	2671	8	2705	79	2686	295	-1
LX-2_Z24_1	4.51	0.73	12.79	43	89	0.1784	0.4	0.5127	1.4	12.6117	1.4	0.95	2638	7	2668	89	2651	313	-1
LX-2_Z24_2	4.77	0.74	13.84	46	96	0.1722	0.5	0.5018	1.2	11.9118	1.3	0.92	2579	8	2621	75	2597	267	-2

	(mV)			Concentration (ppm)		†Ratios							Ages (Ma)						§% disc
Analysis	^{206}Pb	^{207}Pb	^{238}U	Pb	U*	^{207}Pb/^{206}Pb	±1s %	^{206}Pb/^{238}U	±1s %	^{207}Pb/^{235}U	±1s %	Rho	^{207}Pb/^{206}Pb	±2s abs	^{206}Pb/^{238}U	±2s abs	^{207}Pb/^{235}U	±2s abs	
LX11_Z1_1	3.87	0.65	10.21	13	26	0.1979	0.2	0.5125	1.7	13.9815	1.7	0.99	2809	3	2667	113	2748	48	5
LX11_Z1_2	4.75	0.78	12.43	16	32	0.1941	0.2	0.5188	1.5	13.8863	1.5	0.99	2777	3	2694	99	2742	41	3
LX11_Z1_3¶	3.76	0.62	9.64	13	25	0.1952	0.2	0.5249	1.5	14.1293	1.5	0.99	2787	4	2720	99	2758	41	2
LX11_Z1_4	3.67	0.59	9.72	12	25	0.1906	0.2	0.5096	1.5	13.3938	1.5	0.99	2748	4	2655	99	2708	42	3
LX11_Z1_5¶	2.47	0.40	6.45	8	16	0.1934	0.3	0.5243	1.4	13.9850	1.4	0.97	2772	5	2717	91	2749	38	2
LX11_Z2_1	7.98	1.32	21.85	27	56	0.1945	0.1	0.5090	1.4	13.6498	1.4	0.99	2780	2	2653	90	2726	38	5
LX11_Z2_2	5.20	0.86	13.58	18	35	0.1949	0.2	0.5191	1.1	13.9530	1.1	0.99	2784	3	2695	75	2747	31	3
LX11_Z2_3	3.92	0.65	10.50	13	27	0.1949	0.2	0.5139	1.5	13.8118	1.6	0.99	2784	4	2673	102	2737	43	4
LX11_Z2_4	6.24	1.01	16.93	21	43	0.1914	0.2	0.5036	1.1	13.2927	1.1	0.99	2755	3	2629	73	2701	31	5
LX11_Z2_5	3.49	0.56	9.50	12	24	0.1900	0.3	0.5032	1.5	13.1791	1.5	0.98	2742	5	2627	98	2693	42	4
LX11_Z4_1‡	11.62	1.62	89.61	39	229	0.1646	0.4	0.1715	1.7	3.8915	1.7	0.98	2504	6	1020	36	1612	27	59
LX11_Z4_1A‡	6.61	0.91	83.09	22	212	0.1617	0.8	0.1088	2.4	2.4256	2.5	0.95	2474	14	666	34	1250	32	73
LX11_Z5_A	3.83	0.59	8.78	11	22	0.1832	0.3	0.4775	1.4	12.0597	1.4	0.98	2682	4	2516	83	2609	36	6
LX11_Z5_1	4.34	0.68	12.24	15	31	0.1841	0.2	0.4764	1.3	12.0910	1.3	0.98	2690	4	2512	81	2611	35	7
LX11_Z5_2	3.33	0.55	8.83	11	23	0.1949	0.3	0.5072	1.3	13.6325	1.3	0.98	2784	4	2645	82	2725	35	5
LX11_Z5_3	4.23	0.70	11.05	14	28	0.1959	0.2	0.5054	1.3	13.6503	1.3	0.99	2792	3	2637	84	2726	36	6
LX11_Z5_4	0.96	0.09	4.26	3	11	0.1131	1.2	0.3100	1.7	4.8331	2.0	0.82	1849	21	1741	66	1791	36	6
LX11_Z6_A	3.86	0.61	8.81	11	22	0.1866	0.2	0.4857	1.6	12.4960	1.7	0.99	2712	4	2552	102	2642	44	6
LX11_Z6_1	3.96	0.66	10.62	13	27	0.1951	0.2	0.5074	1.5	13.6522	1.5	0.99	2786	4	2646	96	2726	41	5
LX11_Z6_2	3.91	0.61	10.59	13	27	0.1842	0.3	0.4929	1.4	12.5208	1.4	0.98	2691	4	2583	88	2644	38	4
LX11_Z6_3	2.99	0.41	9.40	10	24	0.1623	0.3	0.4439	1.3	9.9360	1.3	0.97	2480	5	2368	72	2429	32	5
LX11_Z7_A	3.69	0.59	8.16	10	20	0.1886	0.2	0.4969	1.3	12.9196	1.3	0.98	2730	4	2601	81	2674	35	5
LX11_Z7_1	1.24	0.18	3.59	4	9	0.1747	0.8	0.4656	1.5	11.2121	1.7	0.89	2603	13	2464	89	2541	43	5
LX11_Z7_2	2.02	0.32	5.55	7	14	0.1881	0.5	0.4804	1.2	12.4566	1.3	0.93	2725	8	2529	76	2639	35	7
LX11_Z7_3	4.45	0.72	12.21	15	31	0.1898	0.2	0.4846	1.6	12.6809	1.6	0.99	2740	3	2547	97	2656	42	7
LX11_Z8_A	2.56	0.38	5.99	7	15	0.1754	0.3	0.4687	1.1	11.3368	1.1	0.96	2610	5	2478	63	2551	28	5
LX11_Z8_1	1.59	0.24	4.61	5	12	0.1767	0.5	0.4604	1.3	11.2177	1.4	0.92	2622	9	2441	74	2541	35	7
LX11_Z8_2	2.77	0.45	7.51	9	19	0.1925	0.3	0.4952	1.3	13.1439	1.3	0.98	2764	4	2593	83	2690	36	6
LX11_Z8_3	3.46	0.57	9.57	12	24	0.1912	0.2	0.4897	1.7	12.9100	1.7	0.99	2753	4	2569	107	2673	46	7
LX11_Z8_4	3.50	0.57	9.48	12	24	0.1932	0.2	0.5059	1.8	13.4788	1.8	0.99	2770	4	2639	114	2714	48	5
LX11_Z8_5	5.42	0.89	14.67	18	37	0.1941	0.2	0.5010	1.4	13.4089	1.4	0.99	2777	3	2618	87	2709	37	6
LX11_Z9_A	2.81	0.45	6.23	8	15	0.1890	0.4	0.4960	1.5	12.9284	1.5	0.97	2734	6	2597	94	2674	41	5
LX11_Z9_1	2.02	0.29	6.22	7	16	0.1685	1.0	0.4316	1.1	10.0294	1.5	0.74	2543	17	2313	62	2437	37	9
LX11_Z9_2	1.95	0.29	5.69	7	16	0.1784	0.4	0.4674	1.3	11.4940	1.4	0.95	2638	7	2472	77	2564	35	6
LX11_Z9_3	3.24	0.53	8.88	7	15	0.1931	0.3	0.5029	1.1	13.3869	1.2	0.98	2768	4	2626	73	2707	32	5
LX11_Z10_A	2.58	0.42	5.69	7	14	0.1911	0.4	0.5034	1.1	13.2643	1.1	0.94	2752	7	2628	69	2699	31	4
LX11_Z10_1	4.98	0.81	13.33	17	34	0.1917	0.2	0.5167	1.4	13.6577	1.4	0.99	2757	3	2685	90	2726	37	3
LX11_Z10_2¶	4.53	0.74	11.99	15	31	0.1917	0.2	0.5200	1.2	13.7405	1.2	0.99	2756	3	2699	81	2732	34	2
LX11_Z11_1	4.32	0.69	11.29	15	29	0.1880	0.3	0.5081	1.2	13.1685	1.3	0.98	2724	4	2649	80	2692	34	3
LX11_Z12_1‡	3.49	0.47	28.67	12	73	0.1570	1.5	0.1795	4.7	3.8868	4.9	0.95	2424	26	1064	107	1611	79	56
LX11_Z13_1¶	4.97	0.82	13.25	17	34	0.1919	0.2	0.5237	1.5	13.8547	1.5	0.99	2758	3	2715	98	2740	40	2
LX11_Z13_2¶	5.12	0.81	13.81	17	35	0.1870	0.2	0.5128	1.7	13.2224	1.7	0.99	2716	3	2669	114	2696	47	2
LX11_Z13_3‡	4.87	0.82	14.97	16	38	0.1988	0.2	0.4454	1.6	12.2087	1.6	0.99	2816	4	2375	88	2621	41	16
LX11_Z14_6	0.48	0.07	1.41	2	4	0.1740	1.3	0.4648	1.2	11.1518	1.8	0.66	2597	22	2461	70	2536	45	5
LX11_Z14_7	0.40	0.06	1.13	1	3	0.1787	1.5	0.4779	1.1	11.7746	1.8	0.59	2641	25	2518	67	2587	48	5
LX11_Z14_8	1.19	0.18	3.40	4	9	0.1767	0.6	0.4734	1.1	11.5325	1.3	0.88	2622	10	2499	68	2567	32	5
LX11_Z18_7	3.41	0.55	9.26	12	24	0.1896	0.2	0.5057	1.9	13.2201	1.9	0.99	2739	4	2638	122	2695	51	4
LX11_Z18_8	0.66	0.09	2.00	2	5	0.1667	1.0	0.4602	1.5	10.5782	1.8	0.83	2525	17	2440	91	2487	46	3
LX11_Z18_9	1.50	0.22	4.28	5	11	0.1738	0.5	0.4650	1.5	11.1461	1.6	0.95	2595	8	2462	90	2535	40	5
LX11_Z18_10	4.61	0.76	12.81	16	33	0.1942	0.2	0.5068	2.4	13.5722	2.4	1.00	2778	3	2643	153	2720	65	5
LX11_Z19_1	1.29	0.21	3.44	4	9	0.1914	0.5	0.5088	1.2	13.4256	1.3	0.91	2754	9	2651	77	2710	35	4
LX11_Z19_2	2.22	0.35	5.92	8	15	0.1897	0.3	0.5083	1.2	13.2949	1.2	0.96	2739	5	2649	75	2701	32	3
LX11_Z20_1	2.85	0.45	7.98	10	20	0.1891	0.3	0.4823	1.7	12.5772	1.7	0.99	2734	5	2537	104	2649	45	7
LX11_Z20_2	3.91	0.64	11.00	13	28	0.1955	0.2	0.4999	1.6	13.4749	1.6	0.99	2789	3	2613	100	2714	43	6
LX11_Z21_1	3.46	0.56	9.57	12	24	0.1942	0.2	0.5032	1.3	13.4723	1.3	0.98	2778	4	2628	82	2713	35	5

	(mV)			Concentration (ppm)		†Ratios							Ages (Ma)						§% disc
Analysis	^{206}Pb	^{207}Pb	^{238}U	Pb	U*	^{207}Pb/^{206}Pb	±1s %	^{206}Pb/^{238}U	±1s %	^{207}Pb/^{235}U	±1s %	Rho	^{207}Pb/^{206}Pb	±2s abs	^{206}Pb/^{238}U	±2s abs	^{207}Pb/^{235}U	±2s abs	
LX-6_Z2_4	15.37	1.55	60.27	81	257	0.1142	0.1	0.3395	1.3	5.3430	1.3	1.00	1867	2	1884	57	1876	133	-1
LX-6_Z2_5	6.42	0.65	25.04	34	107	0.1150	0.2	0.3365	1.2	5.3334	1.2	0.98	1879	4	1870	52	1874	125	1
LX-6_Z2_6	7.73	0.78	28.65	41	122	0.1145	0.2	0.3553	1.3	5.6068	1.3	0.99	1871	3	1960	58	1917	137	-5
LX-6_Z4_1	7.80	1.31	18.41	41	79	0.1874	0.4	0.5199	1.3	13.4330	1.3	0.96	2720	6	2699	85	2711	312	1
LX-6_Z4_2	2.68	0.42	6.56	14	28	0.1767	0.4	0.4990	1.3	12.1611	1.4	0.95	2623	7	2610	84	2617	297	0
LX-6_Z4_3	1.44	0.19	4.20	8	18	0.1537	1.0	0.4334	1.6	9.1854	1.9	0.86	2388	17	2321	91	2357	306	3
LX-6_Z4_4	1.26	0.16	4.00	7	17	0.1432	1.3	0.4006	1.8	7.9100	2.2	0.82	2266	22	2172	93	2221	306	4
LX-6_Z5_1	0.43	0.06	1.15	2	5	0.1621	0.5	0.4557	2.0	10.1877	2.1	0.97	2478	8	2421	116	2452	356	2
LX-6_Z5_2	0.50	0.07	1.31	3	6	0.1613	1.3	0.4730	1.8	10.5174	2.2	0.81	2469	22	2497	107	2481	384	-1
LX-6_Z5_3	0.41	0.06	1.09	2	5	0.1600	1.5	0.4657	2.2	10.2765	2.7	0.82	2456	26	2465	131	2460	447	0
LX-6_Z6_1	3.36	0.41	10.75	18	46	0.1386	1.2	0.3931	1.9	7.5135	2.3	0.85	2210	21	2137	97	2175	296	3
LX-6_Z6_2	6.33	0.69	22.42	34	96	0.1238	0.8	0.3499	1.5	5.9726	1.7	0.87	2011	15	1934	66	1972	186	4
LX-6_Z6_3	3.54	0.44	10.92	19	47	0.1421	0.3	0.3999	1.3	7.8359	1.3	0.97	2253	5	2169	67	2212	193	4
LX-6_Z6_4	3.94	0.57	10.67	21	46	0.1617	0.5	0.4576	1.2	10.2040	1.3	0.93	2474	8	2429	72	2453	243	2
LX-6_Z6_5	2.67	0.38	7.27	14	31	0.1592	0.3	0.4569	1.3	10.0282	1.4	0.97	2447	6	2426	78	2437	247	1
LX-6_Z7_1	0.72	0.10	2.10	4	9	0.1531	0.5	0.4433	1.4	9.3561	1.5	0.94	2380	9	2366	79	2374	248	1
LX-6_Z7_2	1.09	0.15	3.12	6	13	0.1569	0.7	0.4517	1.3	9.7710	1.5	0.89	2422	11	2403	75	2413	254	1
LX-6_Z7_3	1.42	0.18	4.19	8	18	0.1469	0.6	0.4389	1.4	8.8892	1.5	0.92	2310	11	2346	79	2327	246	-2
LX-6_Z7_4	0.46	0.07	1.19	2	5	0.1648	0.5	0.5008	1.5	11.3789	1.6	0.95	2505	8	2617	98	2555	318	-4
LX-6_Z7_5	1.03	0.14	2.97	5	13	0.1568	0.5	0.4541	1.3	9.8162	1.4	0.94	2421	8	2414	77	2418	250	0
LX-6_Z7_6	0.66	0.09	1.82	4	8	0.1596	0.5	0.4739	1.5	10.4283	1.5	0.95	2451	8	2501	89	2474	284	-2
LX-6_Z8_1	2.66	0.37	7.62	14	33	0.1583	0.5	0.4540	1.2	9.9121	1.3	0.93	2438	8	2413	71	2427	236	1
LX-6_Z8_2	2.57	0.36	7.36	14	31	0.1587	0.3	0.4542	1.3	9.9369	1.3	0.97	2441	5	2414	73	2429	234	1
LX-6_Z8_3	3.09	0.44	8.62	16	37	0.1608	0.5	0.4687	1.3	10.3920	1.4	0.93	2464	8	2478	75	2470	251	-1
LX-6_Z8_4	2.84	0.40	8.04	15	34	0.1599	0.3	0.4594	1.2	10.1269	1.2	0.97	2455	5	2437	71	2446	228	1
LX-6_Z10_1A	29.76	3.08	119.11	158	509	0.1170	0.5	0.3268	1.3	5.2734	1.4	0.93	1911	9	1823	53	1865	136	5
LX-6_Z10_2	8.78	0.89	34.00	47	145	0.1152	0.2	0.3357	1.2	5.3330	1.2	0.99	1884	3	1866	52	1874	123	1
LX-6_Z11_1	5.89	0.89	16.36	31	70	0.1713	0.7	0.4645	1.3	10.9721	1.4	0.89	2571	11	2459	77	2521	280	4
LX-6_Z11_2	9.05	1.38	24.96	48	107	0.1710	0.5	0.4729	1.2	11.1473	1.3	0.93	2567	8	2496	76	2536	266	3
LX-6_Z12_1	10.59	1.55	29.89	56	128	0.1648	0.1	0.4625	1.3	10.5060	1.3	1.00	2505	2	2450	79	2480	252	2
LX-6_Z13_1	5.80	0.84	16.48	31	70	0.1629	0.2	0.4632	1.4	10.4047	1.5	0.99	2486	3	2454	86	2471	269	1
LX-6_Z13_2	1.89	0.27	5.31	10	23	0.1621	0.4	0.4544	1.4	10.1543	1.5	0.96	2477	7	2415	83	2449	269	3
LX-6_Z14_1	1.99	0.29	5.74	11	25	0.1611	0.4	0.4506	1.3	10.0119	1.3	0.96	2468	6	2398	72	2436	237	3
LX-6_Z14_2	4.21	0.60	11.48	22	49	0.1621	0.2	0.4669	1.6	10.4365	1.6	0.99	2478	4	2470	94	2474	290	0
LX-6_Z15_1	5.35	0.63	18.36	28	78	0.1327	0.5	0.3772	1.3	6.9020	1.4	0.94	2134	8	2063	63	2099	177	3
LX6-Z15_1B	14.11	2.28	36.60	75	156	0.1826	0.5	0.5097	1.3	12.8325	1.4	0.93	2677	8	2655	83	2667	304	1
LX6-Z15_2	11.37	1.78	30.44	60	130	0.1775	0.2	0.4908	1.4	12.0121	1.4	0.99	2630	4	2574	87	2605	296	2
LX6-Z15_3	9.76	1.44	25.82	52	110	0.1666	0.4	0.4895	1.4	11.2465	1.4	0.97	2524	6	2569	88	2544	286	-2
LX6-Z16_2A	19.67	2.00	79.02	104	337	0.1153	0.1	0.3228	1.4	5.1308	1.4	1.00	1884	2	1803	57	1841	135	4
LX6-Z16_2	6.39	0.64	24.64	34	105	0.1135	0.2	0.3425	1.2	5.3585	1.2	0.98	1856	4	1899	52	1878	123	-2
LX6-Z17_1	5.24	0.88	12.42	28	53	0.1899	0.5	0.5509	1.3	14.4212	1.4	0.93	2741	8	2829	91	2778	342	-3
LX6-Z17_2	7.31	1.25	17.21	39	74	0.1927	0.2	0.5553	1.2	14.7548	1.2	0.99	2766	3	2847	87	2800	317	-3
LX6-Z17_3	3.97	0.65	9.79	21	42	0.1863	0.5	0.5321	1.2	13.6710	1.3	0.93	2710	8	2750	84	2727	314	-1
LX6-Z19_1	8.87	1.37	23.86	47	102	0.1742	0.2	0.4907	1.2	11.7867	1.3	0.99	2598	4	2574	78	2588	263	1
LX6-Z19_2	8.57	1.32	22.17	45	95	0.1733	0.5	0.5057	1.2	12.0863	1.3	0.92	2590	8	2638	78	2611	278	-2
LX6-Z19_3	14.04	2.22	35.33	74	151	0.1792	0.6	0.5086	1.3	12.5653	1.4	0.92	2645	9	2651	82	2648	302	0
LX-6_Z16_3	16.34	1.65	59.92	87	256	0.1156	0.1	0.3492	1.2	5.5636	1.2	0.99	1888	2	1931	53	1910	127	-2
LX-6_Z16_4	1.52	0.16	5.70	8	24	0.1186	0.5	0.3358	1.4	5.4898	1.5	0.94	1935	9	1866	60	1899	152	4
LX-6_Z16_5	7.53	0.77	28.80	40	123	0.1149	0.5	0.3402	1.2	5.3911	1.3	0.93	1879	9	1887	54	1883	136	0
LX-6_Z20_2	0.39	0.05	1.23	2	5	0.1481	0.5	0.4189	1.4	8.5563	1.5	0.94	2324	9	2256	73	2292	226	3
LX-6_Z20_3	0.65	0.07	2.38	3	10	0.1238	1.3	0.3568	1.3	6.0892	1.8	0.72	2011	23	1967	61	1989	206	2
LX-6_Z20_4	2.11	0.23	7.80	11	33	0.1227	0.6	0.3594	1.3	6.0821	1.5	0.92	1996	10	1979	62	1988	166	1
LX-6_Z20_5	0.68	0.09	2.12	4	9	0.1464	0.5	0.4247	1.4	8.5726	1.5	0.94	2304	9	2282	74	2294	226	1
LX-6_Z20_6	1.06	0.13	3.52	6	15	0.1357	1.1	0.3990	1.6	7.4632	2.0	0.83	2173	19	2164	84	2169	262	0
LX-6_Z1_1	0.95	0.10	4.01	8	27	0.1159	1.0	0.3272	0.8	5.2304	1.2	0.62	1894	17	1825	33	1858	124	4
LX-6_Z1_4	2.83	0.29	11.06	25	73	0.1151	0.4	0.3562	1.1	5.6525	1.2	0.94	1881	7	1964	50	1924	126	-4
LX-6_Z1_5	14.47	1.47	61.44	127	407	0.1154	0.2	0.3256	0.8	5.1789	0.9	0.97	1885	4	1817	35	1849	86	4
LX-6_Z1_6	3.38	0.34	13.57	30	90	0.1150	0.3	0.3387	0.9	5.3693	1.0	0.94	1880	6	1880	40	1880	101	0
LX-6_Z1_7	4.71	0.48	18.39	41	122	0.1153	0.3	0.3538	0.7	5.6226	0.8	0.95	1884	5	1953	33	1920	85	-4
LX-6_Z1_8	14.27	1.44	64.33	125	426	0.1150	0.1	0.3049	0.7	4.8369	0.7	0.99	1881	2	1716	28	1791	68	9
LX6_Z1_9	7.45	0.76	29.81	65	197	0.1159	0.5	0.3401	0.6	5.4334	0.8	0.77	1893	9	1887	26	1890	83	0

Table 6

	(mV)			Concentration (ppm)		†Ratios							Ages (Ma)						§% disc
Analysis	^{206}Pb	^{207}Pb	^{238}U	Pb	U*	^{207}Pb/^{206}Pb	±1s %	^{206}Pb/^{238}U	±1s %	^{207}Pb/^{235}U	±1s %	Rho	^{207}Pb/^{206}Pb	±2s abs	^{206}Pb/^{238}U	±2s abs	^{207}Pb/^{235}U	±2s abs	
LX6_T1_1	8.80	1.53	35.16	50	173	0.1900	5.8	0.3213	1.5	8.4185	6.0	0.2581	2742	95	1796	48	2277	103	35
LX6_T1_2	8.38	2.70	25.09	48	123	0.3521	3.1	0.4151	1.6	20.1532	3.5	0.4560	3716	48	2238	60	3099	66	40
LX6_T1_3	8.89	2.58	29.91	51	147	0.3099	7.1	0.3808	2.3	16.2685	7.5	0.3055	3520	110	2080	80	2893	133	41
LX6_T1_4	6.32	1.47	22.96	36	113	0.2617	2.0	0.3571	1.1	12.8853	2.3	0.4868	3257	32	1969	38	2671	43	40
LX6_T1_5	6.28	0.86	26.10	36	128	0.1586	2.0	0.3062	1.1	6.6972	2.3	0.4932	2441	33	1722	33	2072	39	29
LX6_T1_6	9.35	4.14	24.85	53	122	0.4910	3.9	0.4862	2.9	32.9165	4.8	0.5935	4214	57	2554	119	3578	91	39
LX6_T1_7	4.88	1.88	13.73	28	67	0.4351	3.2	0.4608	1.9	27.6457	3.8	0.5174	4035	48	2443	79	3407	71	39
LX6_T2_1	7.72	1.18	31.70	44	156	0.1726	5.3	0.3171	1.0	7.5448	5.4	0.1795	2583	89	1775	30	2178	93	31
LX6_T2_2	5.35	1.13	20.36	31	100	0.2439	7.8	0.3581	1.9	12.0421	8.0	0.2372	3146	124	1973	64	2608	140	37
LX6_T2_3	2.62	0.35	10.83	15	53	0.1503	0.4	0.3182	0.6	6.5922	0.7	0.8549	2349	6	1781	18	2058	12	24
LX6_T2_4	6.74	1.47	24.98	38	123	0.2458	4.9	0.3555	1.4	12.0482	5.1	0.2763	3158	77	1961	47	2608	91	38
LX6_T2_5	8.49	0.98	34.92	48	171	0.1334	0.2	0.3165	0.6	5.8202	0.6	0.9616	2143	3	1773	17	1949	10	17
LX6_T2_6	3.56	0.47	14.32	20	70	0.1546	0.3	0.3228	0.6	6.8799	0.6	0.8969	2397	5	1804	18	2096	11	25
LX6_T2_7	8.28	1.15	33.22	47	163	0.1582	2.2	0.3223	0.7	7.0314	2.3	0.2940	2437	36	1801	21	2115	39	26
LX6_T2_7_A	5.05	0.64	20.62	29	101	0.1470	0.3	0.3159	0.9	6.4053	0.9	0.9473	2312	5	1770	28	2033	16	23
LX6_T2_8	6.77	2.24	20.38	39	100	0.3824	3.4	0.4347	1.2	22.9196	3.6	0.3329	3841	51	2327	47	3224	68	39
LX6_T3_1	5.51	0.63	23.80	31	117	0.1308	0.2	0.3039	0.5	5.4829	0.6	0.9298	2109	4	1711	15	1898	9	19
LX6_T3_2	5.76	0.66	25.12	33	123	0.1315	0.2	0.2995	0.5	5.4288	0.5	0.9378	2118	3	1689	15	1889	9	20
LX6_T3_3	5.56	0.75	23.31	32	114	0.1575	2.1	0.3114	0.7	6.7608	2.2	0.3342	2429	36	1748	23	2081	39	28
LX6_T3_4	5.68	0.68	25.06	32	123	0.1353	0.7	0.3059	0.6	5.7054	0.9	0.6774	2167	12	1721	18	1932	16	21
LX6_T3_5	7.31	0.80	32.30	42	159	0.1260	0.2	0.2962	0.7	5.1463	0.7	0.9703	2043	3	1672	21	1844	12	18
LX6_T3_6	5.57	0.62	25.04	32	123	0.1290	0.2	0.2982	0.6	5.3050	0.7	0.9480	2085	4	1682	19	1870	11	19
LX6_T4_1	1.56	0.25	6.18	9	30	0.1785	0.4	0.3356	1.2	8.2596	1.3	0.9403	2639	7	1865	40	2260	23	29
LX6_T4_2	4.89	0.59	21.11	28	104	0.1363	0.4	0.3109	1.3	5.8425	1.4	0.9582	2180	7	1745	40	1953	24	20
LX6_T4_3	3.55	0.45	14.71	20	72	0.1435	0.3	0.3184	1.2	6.2998	1.3	0.9608	2270	6	1782	37	2018	22	22
LX6_T4_4	2.11	0.31	8.72	12	43	0.1644	0.4	0.3219	1.2	7.2985	1.3	0.9468	2502	7	1799	39	2149	23	28
LX6_T4_5	1.22	0.20	4.70	7	23	0.1843	0.5	0.3406	1.2	8.6544	1.3	0.9122	2692	9	1890	38	2302	23	30
LX6_T5_1	4.01	0.48	17.09	23	84	0.1356	0.4	0.3084	1.2	5.7659	1.3	0.9364	2171	8	1733	36	1941	21	20
LX6_T5_2	5.49	0.63	24.18	31	119	0.1286	0.2	0.2986	1.2	5.2953	1.2	0.9843	2079	4	1684	35	1868	20	19
LX6_T5_3	5.05	0.58	22.59	29	111	0.1282	0.2	0.2980	1.2	5.2665	1.2	0.9813	2073	4	1682	34	1863	20	19
LX6_T5_4	4.88	0.67	20.40	28	100	0.1545	1.4	0.3172	1.2	6.7595	1.8	0.6509	2397	23	1776	36	2080	31	26
LX6_T5_5	5.28	1.26	19.35	30	95	0.2502	6.8	0.3580	2.1	12.3497	7.1	0.2943	3186	108	1973	71	2631	125	38
LX6_T6_1	2.95	0.39	12.01	21	71	0.1496	1.1	0.3173	0.9	6.5438	1.4	0.6201	2341	19	1777	27	2052	24	24
LX6_T6_2	2.91	0.39	11.80	21	70	0.1528	0.3	0.3180	0.8	6.7014	0.9	0.9335	2378	5	1780	26	2073	16	25
LX6_T7_1	5.35	0.62	22.94	38	135	0.1311	0.2	0.3008	0.8	5.4377	0.9	0.9632	2113	4	1695	25	1891	15	20
LX6_T7_2	5.29	0.80	21.17	37	125	0.1704	2.9	0.3171	1.0	7.4514	3.0	0.3175	2562	48	1776	30	2167	53	31
LX6_T7_3	5.43	0.97	21.21	38	125	0.2074	2.8	0.3301	1.0	9.4406	2.9	0.3430	2886	45	1839	32	2382	52	36
LX6_T7_4	6.45	1.93	21.30	46	126	0.3449	3.5	0.3928	1.4	18.6798	3.7	0.3680	3685	53	2136	50	3025	70	42
LX6_T8_1	5.41	0.62	23.28	38	138	0.1313	0.3	0.2987	0.8	5.4074	0.9	0.9267	2116	6	1685	25	1886	15	20
LX6_T8_2	5.37	0.65	21.51	38	127	0.1372	0.2	0.3196	0.8	6.0441	0.9	0.9697	2192	4	1788	26	1982	15	18
LX6_T8_3	5.22	0.63	21.45	37	127	0.1351	0.2	0.3049	0.8	5.6789	0.9	0.9712	2165	4	1716	25	1928	15	21
LX6_T8_4	5.02	0.58	21.42	35	127	0.1315	0.3	0.3013	0.9	5.4651	0.9	0.9466	2119	5	1698	27	1895	16	20
LX6_T9_1	2.70	0.36	10.52	19	62	0.1535	0.4	0.3205	0.8	6.7853	0.9	0.9188	2386	6	1792	26	2084	16	25
LX6_T9_2	3.00	0.40	11.57	21	68	0.1536	0.3	0.3282	0.9	6.9523	0.9	0.9433	2387	5	1830	28	2105	16	23
LX6_T9_3	3.33	0.42	13.61	24	80	0.1434	0.3	0.3111	0.8	6.1539	0.9	0.9443	2269	5	1746	26	1998	15	23
LX6_T10_1_A	2.26	0.36	8.74	16	52	0.1748	0.6	0.3283	0.9	7.9127	1.1	0.8183	2604	10	1830	28	2221	19	30
LX6_T10_1_B	2.04	0.42	7.27	14	43	0.2379	4.6	0.3510	1.1	11.5136	4.8	0.2372	3106	74	1939	38	2566	85	38
LX6_T10_2	5.11	0.60	21.44	36	127	0.1334	0.3	0.3015	0.8	5.5433	0.9	0.9376	2143	5	1698	24	1907	15	21
LX6_T10_3	4.95	0.66	20.61	35	122	0.1505	1.6	0.3053	0.8	6.3360	1.8	0.4680	2352	27	1717	26	2023	31	27
LX6_T11_1	4.65	0.55	19.66	33	116	0.1328	0.4	0.3015	0.8	5.5218	0.9	0.9067	2136	7	1699	25	1904	16	20
LX6_T11_2	1.86	0.28	7.19	13	42	0.1715	0.5	0.3255	0.8	7.6968	0.9	0.8766	2572	8	1817	26	2196	17	29
LX6_T11_3_A	5.54	0.70	22.86	39	135	0.1432	1.1	0.3035	1.0	5.9910	1.5	0.6471	2266	19	1709	29	1975	25	25
LX6_T11_3_B	4.48	0.57	18.52	32	109	0.1421	0.9	0.3020	0.9	5.9180	1.3	0.6908	2253	16	1701	27	1964	22	24
LX6_T12_1	6.80	1.94	21.22	48	125	0.3256	3.4	0.3950	1.6	17.7327	3.7	0.4294	3597	52	2146	58	2975	69	40
LX6_T12_2	6.15	2.42	15.59	44	92	0.4490	1.1	0.5012	1.0	31.0245	1.4	0.6740	4082	16	2619	42	3520	28	36
LX6_T12_3	14.32	8.33	23.70	101	140	0.6428	2.3	0.7468	2.3	66.1909	3.3	0.7000	4608	34	3596	125	4272	63	22

*Accuracy of U concentration is *c* .20%

†Isotope ratios are not common Pb corrected

§% Discordance is measured as ^{206}Pb/^{238}U age relative to ^{207}Pb/^{206}Pb age

	(mV)			Concentration (ppm)		†Ratios							Ages (Ma)						§% disc
Analysis	^{206}Pb	^{207}Pb	^{238}U	Pb	U*	^{207}Pb/^{206}Pb	±1s %	^{206}Pb/^{238}U	±1s %	^{207}Pb/^{235}U	±1s %	Rho	^{207}Pb/^{206}Pb	±2s abs	^{206}Pb/^{238}U	±2s abs	^{207}Pb/^{235}U	±2s abs	
LX7_Z1_1	7.02	1.06	18.40	50	109	0.1714	1.2	0.4707	1.4	11.1266	1.9	0.76	2572	21	2487	58	2534	34	3
LX7_Z1_2	13.10	2.23	31.40	93	185	0.1936	0.2	0.5327	0.9	14.2196	1.0	0.98	2773	3	2753	41	2764	18	1
LX7_Z1_3	8.30	1.45	19.39	59	115	0.1988	0.2	0.5378	1.6	14.7436	1.6	0.99	2817	3	2774	72	2799	30	2
LX7_Z2_1	6.85	0.66	26.97	48	159	0.1096	0.2	0.3238	0.9	4.8940	0.9	0.98	1793	4	1808	29	1801	16	-1
LX7_Z2_2	7.58	0.73	29.55	54	175	0.1096	0.2	0.3192	0.9	4.8220	0.9	0.98	1792	3	1786	28	1789	16	0
LX7_Z2_3	6.93	0.67	27.36	49	162	0.1098	0.2	0.3146	0.9	4.7622	0.9	0.98	1796	3	1764	28	1778	15	2
LX7_Z2_4	6.15	0.60	22.95	44	136	0.1101	0.2	0.3387	0.9	5.1405	0.9	0.97	1801	4	1880	28	1843	15	-4
LX7_Z3_1	8.69	1.35	23.06	61	136	0.1775	0.3	0.4768	1.0	11.6676	1.0	0.95	2629	5	2514	40	2578	19	4
LX7_Z3_2	8.10	1.40	18.25	57	108	0.1971	0.1	0.5587	0.8	15.1803	0.9	0.99	2802	2	2861	39	2827	16	-2
LX7_Z3_3	5.20	0.90	11.50	37	68	0.1991	0.2	0.5654	1.1	15.5238	1.1	0.99	2819	3	2889	49	2848	20	-2
LX7_Z4_1	11.43	1.12	41.72	81	246	0.1116	0.2	0.3474	0.9	5.3455	0.9	0.98	1826	3	1922	29	1876	15	-5
LX7_Z4_2	9.35	1.00	33.52	66	198	0.1212	0.7	0.3507	1.1	5.8611	1.3	0.84	1974	13	1938	38	1955	23	2
LX7_Z5_1	9.69	1.51	24.13	69	142	0.1778	0.4	0.5220	0.9	12.7945	1.0	0.94	2632	6	2708	41	2665	19	-3
LX7_Z6_1	9.16	0.88	35.58	65	210	0.1095	0.2	0.3260	0.9	4.9223	0.9	0.98	1791	3	1819	27	1806	15	-2
LX7_Z7_1	14.32	1.40	55.45	101	328	0.1112	0.3	0.3300	0.9	5.0588	1.0	0.97	1819	5	1838	30	1829	16	-1
LX7_Z8_1	2.52	0.41	6.46	18	38	0.1851	0.3	0.4997	1.0	12.7542	1.1	0.95	2699	5	2612	43	2662	20	3
LX7_Z8_2	2.68	0.46	6.18	19	36	0.1956	0.3	0.5543	0.9	14.9495	0.9	0.96	2790	4	2843	40	2812	17	-2
LX7_Z10_1	6.83	0.67	25.41	48	150	0.1114	0.3	0.3408	0.9	5.2325	0.9	0.95	1822	5	1891	28	1858	15	-4
LX7_Z11_1	6.84	1.16	16.35	48	97	0.1924	0.2	0.5308	0.9	14.0819	0.9	0.98	2763	3	2745	39	2755	17	1
LX7_Z12_1	9.89	1.65	23.25	70	137	0.1898	0.1	0.5345	1.0	13.9872	1.1	0.99	2740	2	2760	47	2749	20	-1
LX7_Z13	12.18	2.01	27.81	95	176	0.1876	0.3	0.5551	0.9	14.3545	1.0	0.95	2721	5	2846	41	2773	18	-5
LX7_Z15	12.67	2.12	29.82	90	176	0.1900	0.1	0.5438	0.8	14.2447	0.8	0.99	2742	2	2799	38	2766	16	-2
LX7_Z17	6.45	1.17	14.34	46	85	0.2049	0.2	0.5700	1.0	16.0982	1.0	0.98	2865	3	2908	48	2883	20	-1
LX7_Z18	10.74	1.43	32.81	76	194	0.1510	0.2	0.4148	0.9	8.6358	0.9	0.98	2357	3	2237	32	2300	16	5
LX7_Z19	9.07	0.87	35.34	64	209	0.1088	0.2	0.3234	0.9	4.8522	0.9	0.98	1780	3	1806	28	1794	15	-1
LX7_Z20	13.08	1.98	32.69	92	193	0.1709	0.6	0.5107	1.0	12.0333	1.2	0.83	2566	11	2660	42	2607	21	-4

*Accuracy of U concentration is *c*.20%

†Isotope ratios are not common Pb corrected

§% Discordance is measured as ^{206}Pb/^{238}U age relative to ^{207}Pb/^{206}Pb age

Table 8

Age (approx)	Locality	Sample number	Event
1670 Ma	Ben Stack	LX6	Post-Laxfordian cooling through titanite closure temperature (600-700 °C)
1750 Ma	Tarbet	LX11	Laxfordian metamorphism
1773 Ma	Badnabay	LX1	Granite emplacement during partial melting of local crust
1793 Ma	Rhiconich	LX7	Granite emplacement during partial melting of local crust
1880 Ma	Ben Stack	LX6	Alkaline granite intrusion
2475 Ma	Badnabay	LX2	Inverian metamorphism
2480 Ma	Tarbet	LX11	Partial melting and Inverian metamorphism
2840 Ma	Tarbet	LX11	Inherited country rock gneiss protolith age

Figure 1

Click here to download high resolution image

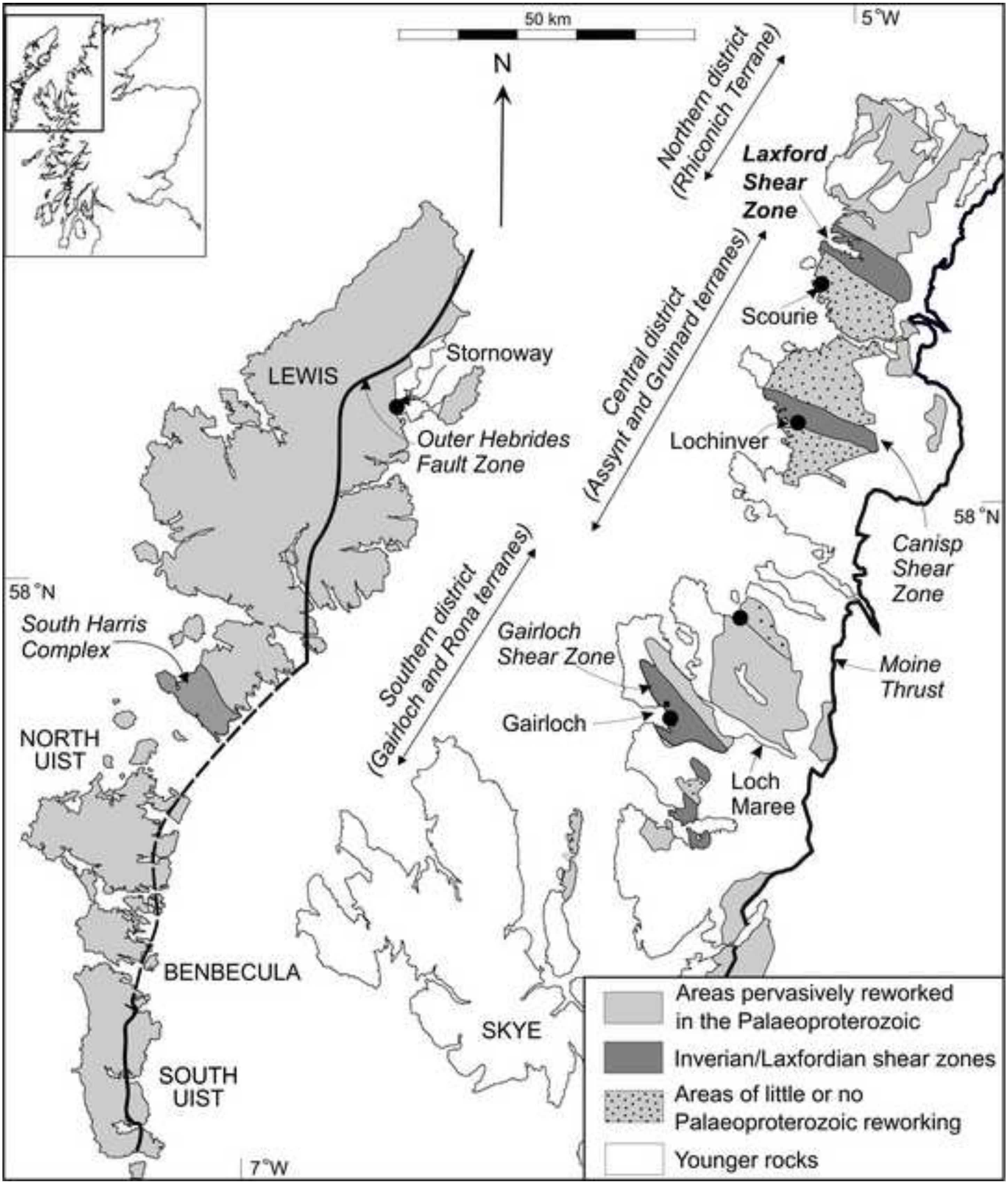

Figure 2
Click here to download high resolution image

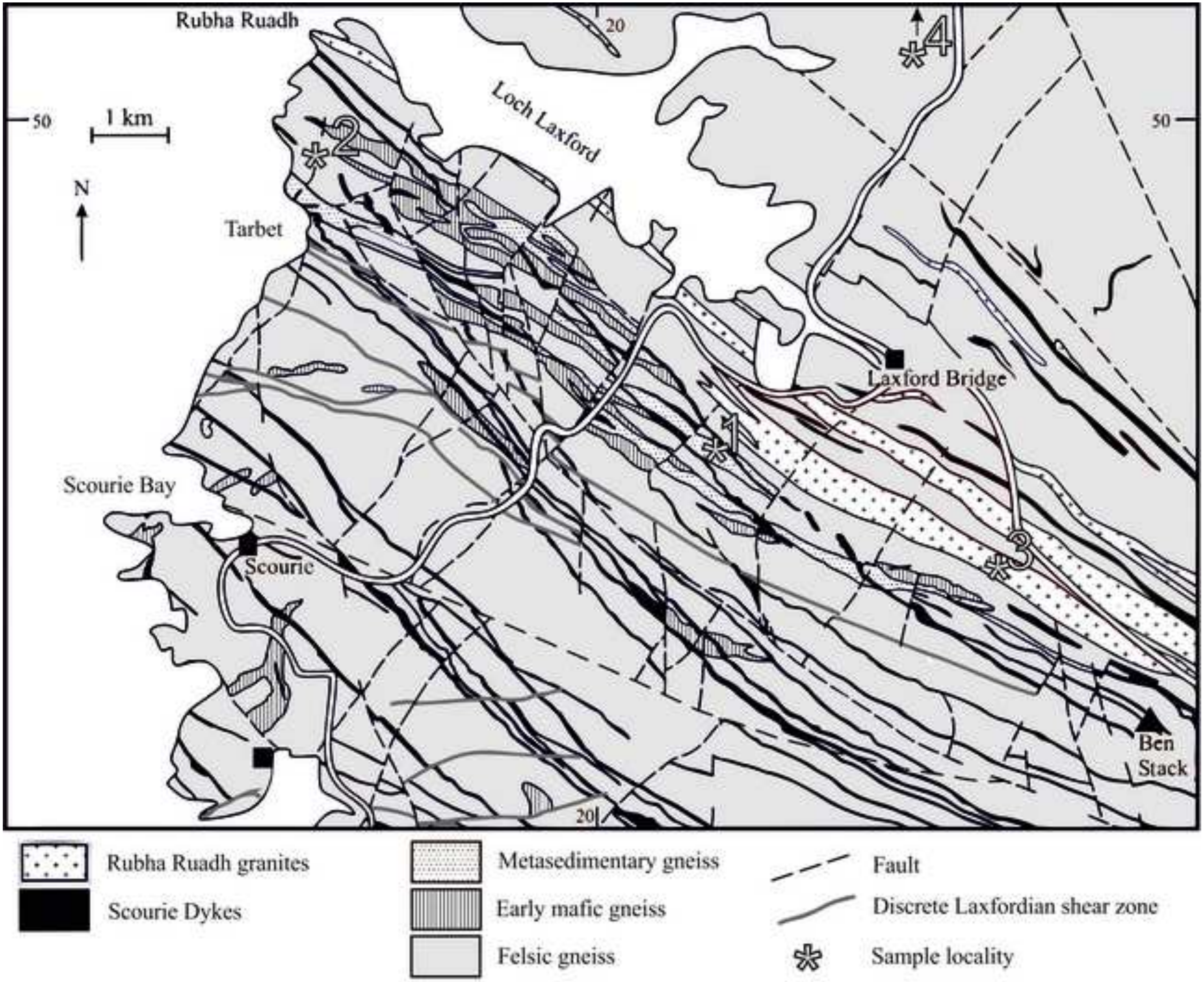

Figure 3
Click here to download high resolution image

Figure4.jpg
Click here to download high resolution image

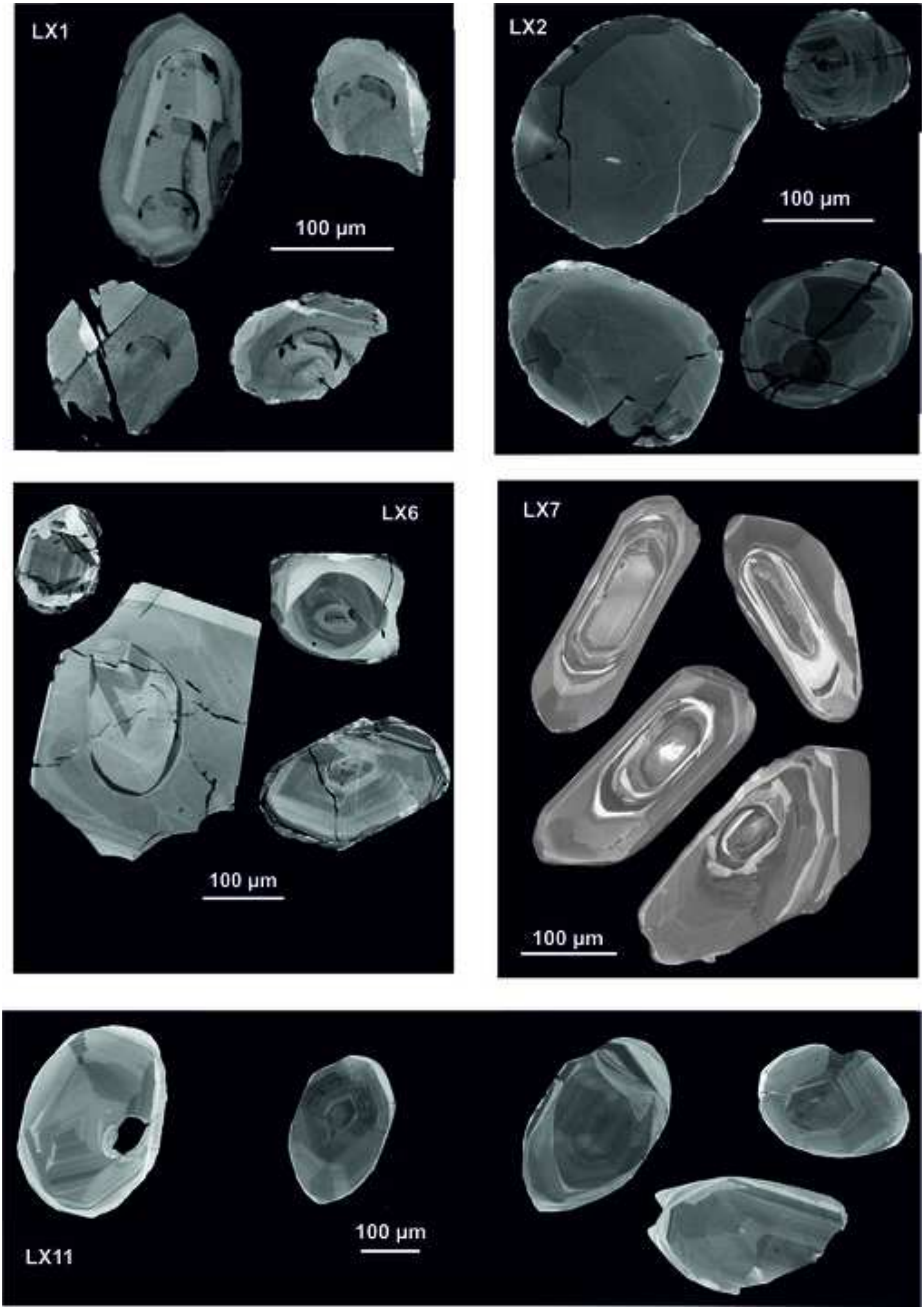

Figure5.jpg
Click here to download high resolution image

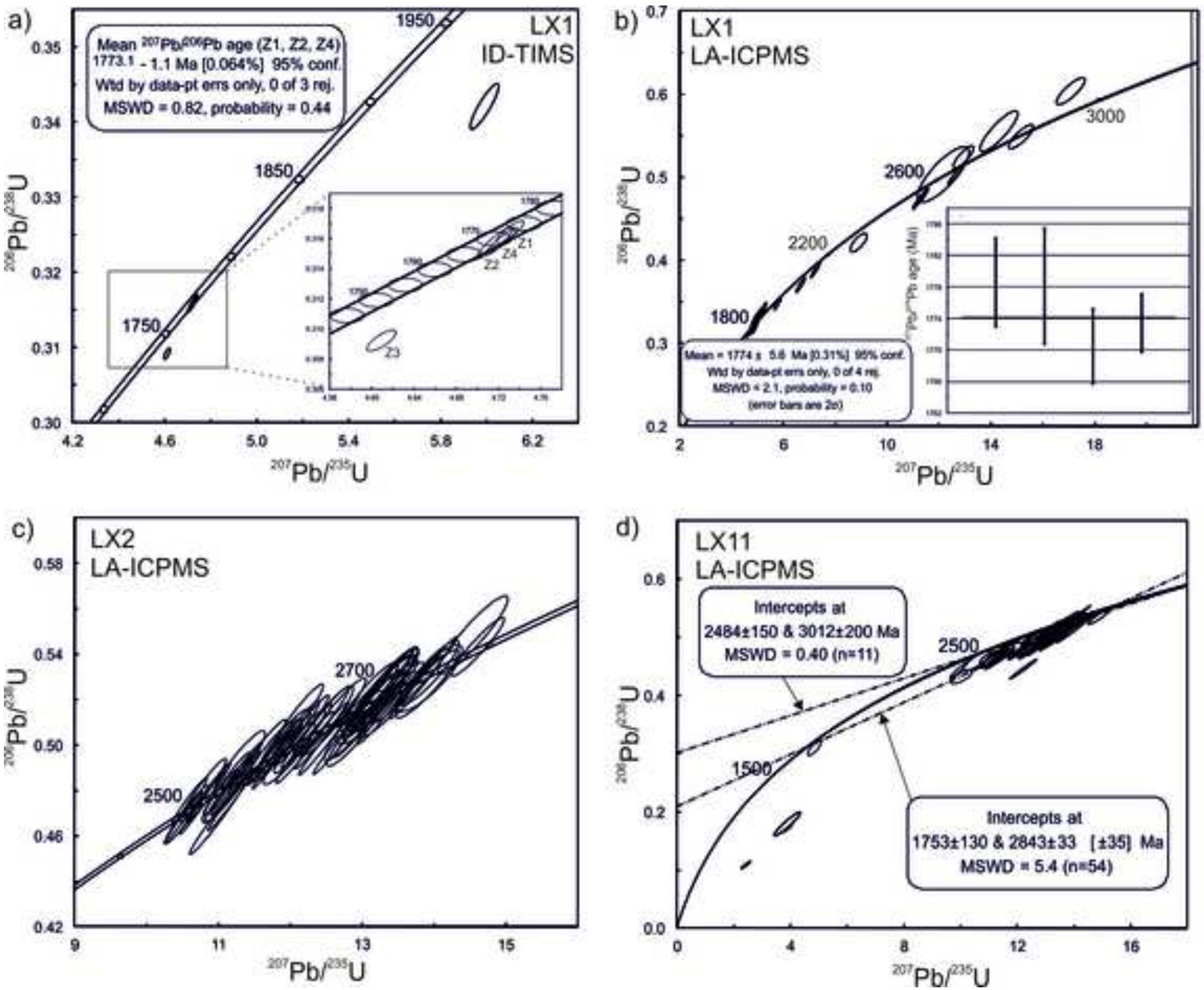

Figure6.jpg
Click here to download high resolution image